



## 저작자표시-비영리-변경금지 2.0 대한민국

이용자는 아래의 조건을 따르는 경우에 한하여 자유롭게

- 이 저작물을 복제, 배포, 전송, 전시, 공연 및 방송할 수 있습니다.

다음과 같은 조건을 따라야 합니다:



저작자표시. 귀하는 원저작자를 표시하여야 합니다.



비영리. 귀하는 이 저작물을 영리 목적으로 이용할 수 없습니다.



변경금지. 귀하는 이 저작물을 개작, 변형 또는 가공할 수 없습니다.

- 귀하는, 이 저작물의 재이용이나 배포의 경우, 이 저작물에 적용된 이용허락조건을 명확하게 나타내어야 합니다.
- 저작권자로부터 별도의 허가를 받으면 이러한 조건들은 적용되지 않습니다.

저작권법에 따른 이용자의 권리는 위의 내용에 의하여 영향을 받지 않습니다.

이것은 [이용허락규약\(Legal Code\)](#)을 이해하기 쉽게 요약한 것입니다.

[Disclaimer](#)

Thesis for the Degree of Master of Science

**Investigating spatiotemporal variability  
of air pollutants in urban areas  
based on a highly dense  
cost-effective sensor network and  
mobile monitoring**

by

Yongmi Park

Department of Environmental Atmospheric Sciences

The Graduate school

Pukyong National University

August 2020

# Investigating spatiotemporal variability of air pollutants in urban areas based on a highly dense cost-effective sensor network and mobile monitoring

(고해상도 저비용 센서 네트워크  
모니터링 및 이동 측정에 의한  
도심 대기오염물질의 시공간 변동  
분석)

Advisor: Prof. Wonsik Choi

by  
Yongmi Park

A thesis submitted in partial fulfillment of the requirements  
for the degree of

Master of Science

in Department of Environmental Atmospheric Sciences, The Graduate  
School,  
Pukyong National University

August 2020

Investigating spatiotemporal variability of air pollutants in  
urban areas based on a highly dense  
cost-effective sensor network and mobile monitoring

A dissertation

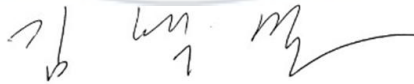
by  
Yongmi Park

Approved by:

A handwritten signature in black ink, appearing to read '김재진' (Kim Jae-jin), is written over a large, faint circular watermark of Pukyong National University.

---

(Chairman) Jae-Jin Kim

A handwritten signature in black ink, appearing to read '백민김' (Baek-min Kim), is written below the signature of the chairman.

---

(Member) Baek-Min Kim

A handwritten signature in black ink, appearing to read '최원식' (Choi Wonsik), is written below the signature of the member.

---

(Member) Wonsik Choi

August, 2020

# Contents

List of Figures .....	iii
-----------------------	-----

List of Tables .....	vii
----------------------	-----

Abstract .....	viii
----------------	------

## CHAPTER 1

INTRODUCTION .....	1
--------------------	---

## CHAPTER 2

COMPARISON OF TRANSIT USER'S INHALATION RATES OF PM <sub>2.5</sub> BETWEEN TRANSPORTATION TYPES .....	
--	--

2.1. Monitoring site .....	6
----------------------------	---

2.2. Meteorological conditions .....	12
--------------------------------------	----

2.3. Temporal distribution according to transportation types .....	14
--	----

2.4. Difference in concentration by transportation types .....	17
--	----

2.5. Inhalation rate according to ventilation rate .....	21
--	----

2.6. Summary .....	25
--------------------	----

## CHAPTER 3

### A HIGHLY DENSE COST-EFFECTIVE SENSOR NETWORK

3.1. Monitoring site .....	27
3.2. Meteorological conditions .....	35
3.3. Temporal distribution .....	41
3.4. Spatial variability .....	52
3.5. Summary .....	55

## CHAPTER 4

CONCLUSIONS .....	57
REFERENCE .....	58

# List of Figures

- Fig. 2.1** Sampling route. Red star represents the locations of air quality monitoring station (AQMS), white lines denote walking route, yellow line represents on-board route for bus (DY→SM) and subway (SM→DY). The blue star represents an intersection. .... 8
- Fig. 2.2** Comparison of PM<sub>2.5</sub> concentrations measured with DustTrak 8530 (DT) and light scattering sensor calibrated ( $R^2 = 0.96$ ) to the instrument with federal equivalent method (FEM) in real atmospheric environments. Black line shows a linear fit with  $R^2 = 0.81$  (calibrated sensor= $0.84 \times [DT] + 1.86$ ) and gray dashed line is 1:1 line. .... 11
- Fig. 2.3** Time-series of PM<sub>2.5</sub> concentrations for sampling periods. Red lines represent the walk along roadside, orange lines in-cabin of buses, yellow lines underground subway station, blue lines platform, and green lines in-cabin of subway train. X-axis is time in seconds with the departure = 0 s. (a) Time-series obtained in May of 2017 (17:00 – 18:30 LT). (b) and (c) show time-series for four different periods of a day on July 27 and August 1 of 2017, respectively. Gray horizontal lines represent the upper limits for good (solid), normal (dotted), and bad (dashed) PM<sub>2.5</sub> conditions. .... 16
- Fig. 2.4** (a) Comparison plot of PM<sub>2.5</sub> levels measured between inside the transportation vs. walk outside. Stars indicate the PM<sub>2.5</sub> levels inside the

subway, Black circles inside the A/C non-operated buses, and gray circles inside the A/C operated buses. Black solid line shows the linear fit for the inside subway ( $R^2 = 0.92$ ), dashed line for A/C non-operated buses ( $R^2 = 0.91$ ).  
 (b) 1:1 plots of  $PM_{2.5}$  concentrations between specific locations of subway and ambient outside. In-cabin of the subway train ( $R^2 = 0.91$ ), at the platform ( $R^2 = 0.76$ ), station (underground,  $R^2 = 0.85$ ). ..... 20

**Fig. 2.5** Decreases in inhaled  $PM_{2.5}$  in the cabin of subways and buses as a function of ambient  $PM_{2.5}$  levels. Inhalation rates of  $PM_{2.5}$  in the cabin ( $[InhalR]_{cabin}$ ) over the rates of the walk along the roadside ( $[InhalR]_{walk}$ ). ([Inhalation rates in cabin]-[Inhalation rates in walk]): fitting equations are -  $0.016 \times [PM_{2.5}] + 0.06$  for A/C operated buses (grey dotted line); -  $0.013 \times [PM_{2.5}] + 0.04$  for subway (black solid line);  $-0.010 \times [PM_{2.5}] + 0.03$  for A/C non-operated buses (gray dashed line). ..... 24

**Fig. 3.1** Satellite image for the monitoring domain including spatial scales of the domain. The yellow box indicates the observation site in the  $800\text{ m} \times 800\text{ m}$  in Seoul. The red star represents the Air Quality Monitoring Station (AQMS), and the blue star represents the Automatic Weather Station (AWS) location within 2 km in the observation site. (1) Site 1 (Eulji-ro); (2) Site 2 (Sogong-ro); (3) Site 3 (Deoksugung-gil) (4) Site 4 (Namdaemun-ro). ..... 28

**Fig. 3.2** Image of the sensor assembly. .... 28



**Fig. 3.3** Results of the comparison between AQMS and unadjusted sensor data for summer and winter (hourly averaged data): in summer (a) CO, (c) NO<sub>2</sub>, (e) O<sub>3</sub>, (g) PM<sub>2.5</sub>; in winter (b) CO, (d) NO<sub>2</sub>, (f) O<sub>3</sub>, (h) PM<sub>2.5</sub>. Red line represents raw data and blue line indicate corrected data. The black dotted lines denote AQMS data. .... 34

**Fig. 3.4** The wind speed and wind direction of the ground and the upper layer (using 5min data). The wind speed range used the Beaufort wind force scale. The left panel is the ground AWS, the right panel is KMA, AWS. (a) Windrose in summer, (b) Windrose in winter. .... 38

**Fig. 3.5** Wind direction/wind speed comparison of the upper layer (KMA, AWS) and the ground (summer: Site 1, winter: Site 2) in the vertical direction. The gray 'x' represents the case where the wind speed is weaker than 0.3 m/s and there is no wind direction. (a) In the summer, it was divided based on the wind direction of the upper wind direction. The black line represents the linear line ( $R^2 = 0.47$ ,  $WS_{KMA,AWS} = 1.8 WS_{ground}$ ) between the KMA, AWS wind speed and ground AWS when the upper wind is the main wind (Northeasterlies). (b) In winter, it was divided based on the wind direction of the ground. The black line represents the linear line ( $R^2 = 0.98$ ,  $WS_{KMA,AWS} = 1.9 WS_{ground}$ ) between the KMA, AWS wind speed and ground AWS when the main wind is on the ground (Northerlies). .... 40

**Fig. 3.6** Box plot of daily changes by measured pollutants by observation area. Each box is the lower 25%, 50%, 75% of the concentration observed during each

day in each Site. The gray shaded part represents the day of precipitation. The blue dotted line indicates the average concentration value of AQMS. The red shaded part represents the day of high  $PM_{2.5}$  concentration event. ....45

**Fig. 3.7** The wind speed and pollutants concentration comparison when the ground wind direction and the upper wind direction coincide with the road direction (the wind speed comparison plot that when the wind direction coincides with the north wind and the northwest wind in winter (considering monsoon, except high  $PM_{2.5}$  con. Day and weekend). (a) CO, (b) NO<sub>2</sub>, (c) O<sub>3</sub>, (d)  $PM_{2.5}$ . ....46

**Fig. 3.8** The average between summer and winter traffic fleet on weekdays. (a) Site 1, (b) Site 2, (c) Site 4. ....47

**Fig. 3.9** Daily variation of contaminants in Site 1 (brown), Site 2 (black), and Site 3 (yellow-green) over the weekday summer observation period (1 hour avg). (a) CO; (b) NO<sub>2</sub>, (c) O<sub>3</sub>; and (d)  $PM_{2.5}$ . ....50

**Fig. 3.10** Daily variation of pollutants in Site 1 (brown), Site 2 (black), Site 3 (yellow-green), and Site 4 (blue) over the weekday winter observation period (1 hour avg). (a) CO; (b) NO<sub>2</sub>, (c) O<sub>3</sub>; and (d)  $PM_{2.5}$ . ....51

**Fig. 3.11** A daily (24h) COD distribution with a concentration of pollutants using 1 h data in observe periods (except for the day when precipitation and high concentrations occurred). Based on Site 3, the circle is the comparison of Site 1, Site 2, Site 2, and the product table, Site 4. Gray is the summer observation and blue are the winter observation. (a) CO, (b) NO<sub>2</sub>, (c) O<sub>3</sub>, (d)  $PM_{2.5}$ . ....54

# List of Tables

<b>Table 2.1</b> Measurement schedule.....	9
<b>Table 2.2</b> Meteorological factors for sampling periods. ....	13
<b>Table 2.3</b> Inhalation rates ( $\mu\text{g}/\text{m}^3$ ) estimated for the in-cabin of the subway and buses, and the walk outside for the sampling periods. ....	23
<b>Table 3.1</b> Each road characteristic and observation period. ....	29
<b>Table 3.2</b> Sensor specifications. ....	32
<b>Table 3.3</b> Results of linear regression between 29 sensors and the reference sensor in summer and winter (using 15-minute averaged unadjusted data). The reference sensor represents the sensor node that was co-located with FRM/FEM instruments at AQMS (Park et al., 2020). ....	33
<b>Table 3.4</b> Meteorological conditions. ....	39

고해상도 저비용 센서 네트워크 모니터링 및  
이동 측정에 의한 도심 대기오염물질의 시공간 변동 분석

박용미

부경대학교 대학원 환경대기학과

요 약

도로환경이 집약적인 형태를 띠면서 단위 면적당 많은 양의 미세먼지를 배출하고 있다. 도로 이동오염원으로부터 직접 배출되는 대기오염물질의 분포는 시간과 공간에서 상당히 비 균질하게 분포되어 있고 이로 인해 공간의 구조와 시간에 따라 보행자 노출 수준에 영향을 미칠 수 있다. 따라서 인구 밀집 도시 지역의 건축 환경에서 대기 오염물질의 공간 분포의 특성을 이해하는 것이 중요하다.

구 단위의 도시대기관측소(Air Quality Monitoring Station, AQMS) 보다 더 상세한 국지적인 데이터 수집을 위하여 이동식 PM<sub>2.5</sub> 측정기기(DUSTTRAK II 모델 8530)를 사용하여 교통량이 많은 도심의 특정 노선을 버스와 지하철을 이용하여 왕복하고 일부는 보행을 통하여 외부노출 정도를 평가하였다. 평균 PM<sub>2.5</sub> 농도는 A/C 이 운행하지 않는 버스 ( $27.1 \mu\text{g}/\text{m}^3$ )의 내부에서 가장 높았다. 건강한 성인을 기준으로 PM<sub>2.5</sub> 질량 농도를 사용하여 흡입량을 추정했으며, 주변 PM<sub>2.5</sub> 농도가  $35 \mu\text{g}/\text{m}^3$  인 경우, A/C 버스, 지하철 및 Non A/C 버스의 내부에서 흡입량이 46 %, 68 % 및 81%로 감소했다.

교통배출량(예: 교통량, 속도, 구성, 유지보수 등) 뿐만 아니라 대기 오염물질 분포에서 공간적 이질성을 제어하는 주요 요인으로는 주변 건축 환경 및 기상 조건이 포함된다. 본 연구에서는  $800 \text{ m} \times 800 \text{ m}$  공간규모의 서울 중심의 관측지역에서 대기오염물질(O<sub>3</sub>, NO<sub>2</sub>, CO, PM<sub>2.5</sub>) 농도의 공간 분포를 조사했으며, 저비용 센서 노드를 사용해 관측지역 내 교통량, 건물

분포 등의 뚜렷한 특징을 가진 4 개의 세부 도심환경 속에서 관측을 진행했다. 공간 변동성을 파악하기 위해 coefficient of divergence (COD) 분석을 사용하였고, 분석 결과는  $PM_{2.5}$  를 제외한 오염물질은 시간과 공간 분포에서 상당히 비균질함을 보였다. CO 와  $NO_2$  는 풍속, 교통량에 영향을 받아 구역마다 농도 차이를 보였다.  $PM_{2.5}$  의 경우 상세 구역내 농도 변화는 거의 없었다.



# CHAPTER 1

## INTRODUCTION

Air pollutants are emitted directly from various sources like vehicles, industrial activities and power plants and formed secondarily in the atmosphere via chemical reactions. Many studies have reported a long list of adverse health effects due to long- and short-term exposure to various primary and secondary air pollutants (Wu et al., 2016; Bentayeb et al., 2015; Hoek et al., 2013). Recent toxicological and epidemiological studies have demonstrated that fine particles are closely linked to various human diseases and mortality (Xing et al., 2016; Sioutas et al., 2005). These studies suggested that  $PM_{2.5}$  causes asthma and respiratory inflammation, and that  $10 \mu g \cdot m^{-3}$  increases in  $PM_{2.5}$  can lead up to 9% increase in lung cancer incidence and 30% - 80% increases in mortality rates of ischemic heart diseases. In addition, Baumgartner et al. (2014) reported that people living near major emission sources such as major roadways in the city center are at high risks of acute and chronic adverse health effects.

Most of particulate pollutants emitted from vehicular sources are  $PM_{2.5}$ , accounting for 92% of the total particles emitted (ME, 2016). Nitrogen oxides from vehicular emissions are oxidized in the atmosphere to be converted into condensed phase, producing  $PM_{2.5}$ , which, in the metropolitan areas, account for about two-thirds of the total produced  $PM_{2.5}$  (ME, 2016; Kim et al., 2014; Morawska et al., 2008).

As a result, pedestrians and public transportation users are exposed to air pollutants emitted from vehicles.

Previous studies have shown that concentrations of air pollutants may vary significantly even within a city due to various controlling factors including urban configuration, micro-built environments, density of traffic networks, fleet composition, land-uses, meteorological conditions, and others (Tan et al., 2014; Britter & Hanna, 2003; Vachon et al., 2002). The wind fields and dispersion characteristics of the in-canopy atmosphere are modified by the urban environments, which alter the capacity of ventilation and dilution of local emissions, ultimately enhancing or mitigating local concentrations of air pollutants near the sources (Britter & Hanna, 2003). Vachon et al. (2002) reported that vehicle-induced turbulence contributes to the turbulent kinetic energy in the lower part of the street canyon, and traffic congestion due to an extraordinarily high traffic density produces less turbulent energy lessening the capacity for pollutants dispersion. Thus, the spatial heterogeneity of air pollutants distributions can affect the levels of pedestrian exposure to air pollutants depending on routes they take within the city. Therefore, it is important to understand the characteristics of the spatial distributions of air pollutants in various micro-built environments particularly in densely populated urban areas.

Currently, the Korean government has established and been operating air pollution monitoring networks since 1989. each monitoring station covers at most 2 - 10 km (NIER, 2019). As of December 2019, the national urban air quality monitoring network consists of 405 air quality monitoring stations (AQMS) (NIER,



2019). However, AQMS are not uniformly distributed over Korea, concentrated in a few megacities, and sparsely located in the other regions. In a composite study analyzing the distributions of traffic-related pollutants with distance from the roads, Karner et al. (2010) showed that the concentrations of pollutants emitted from vehicles decrease as the distance from the road decreases, and that most of pollutants concentrations reach to the background within 160 – 400 meters. (Gaseous pollutants). Dilution by ambient air has the greatest effect on changes in number concentration and size distribution (Kumar et al., 2011b). In stable atmosphere, particle dynamic evolution also has a significant effect such as flocculation/evaporation by particle motion (Kerminen et al., 2007). Therefore, the spatial resolution of the AQMS network even in Seoul is not enough to understand the spatial distributions of pollutant concentrations in various urban micro-environments.

The road environment is intensive and emits a high PM<sub>2.5</sub> concentration per unit area (ME, 2016). As a result, pedestrians and public transport users are exposed to various vehicle emissions pollutants due to non-emission PM emissions such as tire/brake abrasion and road damage, as well as pollutants emitted from vehicles (Kumar et al., 2014; Kumar et al., 2013). The spatial distribution of PM<sub>2.5</sub> mass concentrations in site showed homogeneous regardless of the season. However, the average daily commuting time is only 1.43 hours (Zacharias et al., 2014), but 45 - 50% of people's exposure to ultrafine particles in a day occurs in commuting vehicles (Zhu et al., 2007). Also, the time spent at an intersection is only 2% of commuting time but considering previous studies that particle concentration exposure at an intersection can contribute up to 25% of total commuting time exposure (Goel and Kumar, 2015).



Thus, quantitative evaluation of exposure to fine dust on or near the road is necessary. In chapter 2, pedestrian exposure to  $PM_{2.5}$  was investigated in various environments, estimating quantitatively the amount of  $PM_{2.5}$  inhaled by walking and public transportation users while an individual is traveling by walk, buses, and subways in the real atmospheric environments. The study's goal is to quantitatively estimate the actual amount of  $PM_{2.5}$  inhaled during traveling activities by various ways of transportation and to find effective ways to reduce pedestrian exposure to  $PM_{2.5}$  during transportation in different ambient  $PM_{2.5}$  levels, seasons, and in-cabin conditions.

One emerging solution to understand the spatial heterogeneity of air pollutants distributions that cannot be observed with the current AQMS network is to build a highly spatially resolved air quality monitoring network employing a massive number of low-cost sensors. Recent studies have shown the potential of the low-cost and real-time sensor by using to build high-density sensor networks (Cordero et al., 2018; Spinelle et al., 2015; Mead et al., 2013; Park et al., 2020). The low-cost sensor nodes used in this study were evaluated for consistency between the sensor nodes with intercomparison tests placing 30 sensor nodes in the same place under real atmospheric conditions. They were also evaluated for accuracy by installing them next to the air intake at the AQMS in the center of Seoul and comparing them with reference instruments (Park et al., 2020). The consistency between 30 sensor nodes was great, with  $R^2 > 0.93$ . In addition, the readings from the sensor nodes agreed very well with those of the instruments with federal reference methods (FRM) with  $R^2$  values of 0.87 or higher. These results show that adequately chosen low-cost sensors

can be useful for building high-resolution air quality monitoring networks in complex urban environments with spatially and temporally heterogeneous pollutants (Park et al., 2020; NIER, 2017).

The major factors controlling spatial heterogeneity in the distribution of air pollutants in the urban center include traffic emissions (e.g., traffic volume, speed, composition, maintenance, etc.) and surrounding building environments and weather conditions. In this study, low-cost sensor nodes were used to examine the characteristics of air pollutant concentration distributions in the city center, around Seoul City Hall, the most populated and largest megacity in Korea. Ozone ( $O_3$ ), nitrogen dioxide ( $NO_2$ ), carbon monoxide (CO), particulate matter less than  $2.5\ \mu m$  ( $PM_{2.5}$ ), and less than  $10\ \mu m$  ( $PM_{10}$ ) were measured at intervals of 10 seconds, as well as temperature and humidity. The monitoring area is 800 m by 800 m in space and includes several specific micro-built environments: a street canyon, a mixture of high and low buildings, open space, and AQMS.

## CHAPTER 2

### COMPARISON OF TRANSIT USER'S INHALATION RATES OF PM<sub>2.5</sub> BETWEEN TRANSPORTATION TYPES

#### 2.1. Monitoring site

We measured the PM<sub>2.5</sub> concentration by carrying the PM<sub>2.5</sub> measuring device and moving the specific route repeatedly. Exposures of PM<sub>2.5</sub> were assessed according to the means of transport, including various methods of transportation, such as buses, subways, and walking. The measurement path is as follows. (1) From Pukyong National University (PKNU, DY) to the bus stop located at the front main entrance of the university (in the campus; about 460 m), (2) get on the bus from DY and get off the bus from SM (in the bus; about 5.7 km), walk to SM subway station through the sidewalk adjacent at the boulevard (about 200 m), (3) to the platform through the underground station (underground), (4) Riding on the subway to DY stations (in subway cabin; about 6 km) and (5) returning on foot from the subway station to the starting point (Fig. 2.1).

The measurement route was chosen from Busan, where a lot of traffic and the subway and bus routes were generally matched with about 7 km between DY and SM (Fig. 2.1). There are no large industrial or industrial complexes around the measurement path. Based on the 2018 traffic volume survey, the vehicle speed and traffic volume in the measured path have a difference by section (Fig. 2.1; BMC,

2019). The measurement path was divided into three sections. The average vehicle speed is 21.4 km/hr in section 1 (intersection 1-2) on a weekday, section 2 (intersection 2-3) recorded 27.3 km/hr and section 3 (intersection3-SM) recorded 20.6 km/hr. The first and second sections showed similar vehicle flow, and traffic was frequent at speeds of less than 15 km/hr during rush hour in section 3. The highest traffic was from intersection 2 to intersection 3 (2600 vehicles/hr) and then follows interception 2 to SM (871 vehicles/hr), PKNU to interception 2 (740 vehicles/hr). In case of walking, there was limited vehicle emissions within PKNU, but there was direct exposure from the road during the waiting time at the bus stop, and there was direct exposure from the road by walking along the eight-lane road to the subway station after getting off at SM. When we measured in a bus, the window was checked for opening and closing and was determined whether there was an inflow of outside air. we measured in the subway, it was divided into underground stations of subway stations, platforms, and subway cabin.

Measurements were made for a total of seven days over May (5 days) and July 27, August 1 in 2017. In the spring, the focus was on evening rush hour, with a large floating population and increased traffic. In the summer, it measured a total of four times in daily, including the early morning hours, morning rush hour, afternoon and evening rush hour (Table 2.1). Observations were performed by researchers carrying and moving PM<sub>2.5</sub> observation devices directly to determine PM<sub>2.5</sub> exposure levels and inhalation levels. PM<sub>2.5</sub> The measuring instrument used DUSTRAK TM II Model 8530 (TSI, USA).

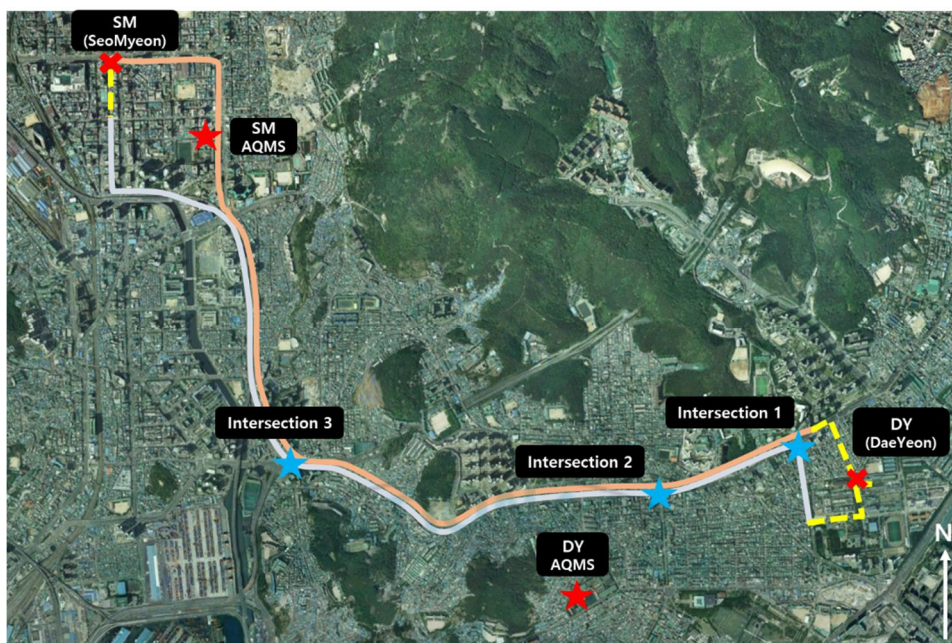


**Fig. 2.1** Sampling route. Red star represents the locations of air quality monitoring station (AQMS), white lines denote walking route, yellow line represents on-board route for bus (DY→SM) and subway (SM→DY). The blue star represents an intersection.

**Table 2.1** Measurement schedule

Date	Time
7/27, 8/1	5:00-6:30
	7:30-9:00
	14:00-15:30
5/11, 5/12, 5/16, 5/23, 5/26, 7/27, 8/1	17:00-18:30





This model is a single channel device that records the mass concentration of aerosols in time using a light scattering method. DUSTRAK (DT) has been widely used in mobile observational studies because its time resolution is very fast and easy to carry in 1 second (Choi et al., 2012; Wang and Gao, 2011). In this study, PM<sub>2.5</sub> was measured by attaching a PM<sub>2.5</sub> impactor (0.1–2.5µm) to the air inlet of the DT. Using HEPA filters, zeroing of the measuring instrument was corrected prior to the start of each observation to minimize the effect of a change in the characteristics of the instrument (Zero check) (Choi et al., 2012). Generally, light scattering devices tend to overestimate concentrations over expensive reference equipment and are known to overestimate more at relative humidity of 60% or more (NIER, 2009). In this study, concentrations were corrected using the correction factor (Ambient Cal. Mode) (TSI, 2019) that the manufacturer suggested could be applied to the actual atmosphere. Although it is not a reference equipment, DT has corrected through light scattering method sensors (PMS 5003, Plantower) that were calibrated through comparison observations with the reference equipment and the actual atmospheric conditions ( $R^2 = 0.955$ ; Park et al., 2020). As a result, if the actual concentration lower, DT was underestimation, and the higher the concentration, DT was to overestimate (Fig. 2.2). However, considering that the concentration in the atmosphere during the measurement period was lower than 20 µg/m<sup>3</sup>, the concentration of DT was consistent within ±1.75 µg/m<sup>3</sup> (15%) with the sensor concentration corrected by reference equipment. Thus, the accuracy of the data is thought to be appropriate.

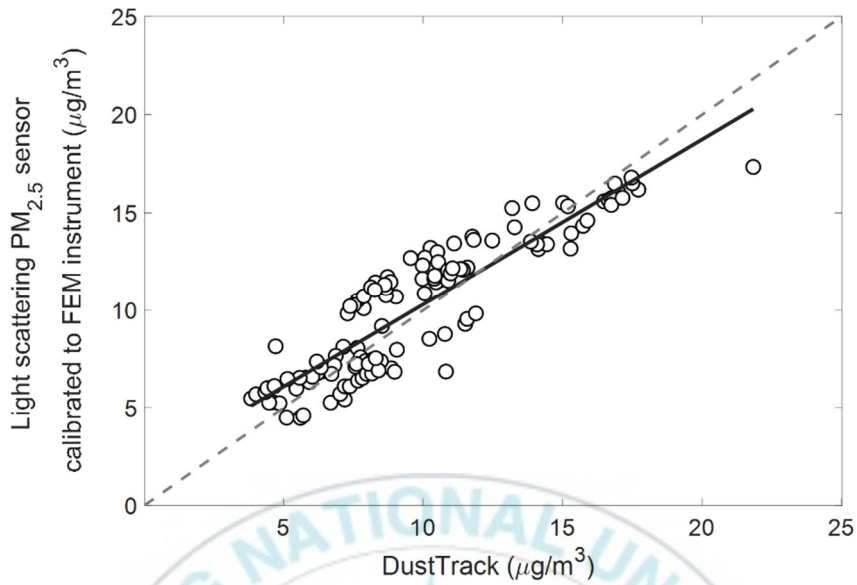


**Fig. 2.2** Comparison of  $\text{PM}_{2.5}$  concentrations measured with DustTrak 8530 (DT) and light scattering sensor calibrated ( $R^2 = 0.96$ ) to the instrument with federal equivalent method (FEM) in real atmospheric environments. Black line shows a linear fit with  $R^2 = 0.81$  (calibrated sensor =  $0.84 \times [\text{DT}] + 1.86$ ) and gray dashed line is 1:1 line.



## 2.2. Meteorological conditions

Temperature, wind speed, and wind direction data were obtained from the Automatic Weather System (AWS) of DY in Busan, and the humidity was used as the average daily data in KMA, AWS from Busan. PM<sub>2.5</sub> concentrations representing the region were used for data from AQMS DY (Fig. 2.1) and AQMS SM (Fig. 2.1) of Air Korea. During the measurement period, the overall humidity was high at an average of 70%, and the wind speed was weakly blown below 3 m/s. In May, wind was predominantly blown in the south-easterlies, and in July and August, the wind direction was recorded east. On May 11, the average concentration of PM<sub>2.5</sub> in all AQMS in Busan was 46 µg/m<sup>3</sup>, and the overall concentration in Busan was high concentration.

**Table 2.2** Meteorological factors for sampling periods.

Date	Time	Temp. ( )	Humid (%)	Wind speed (m/s)	Wind direction ( )	PM <sub>2.5</sub> (μg/m <sup>3</sup> ) <sup>#</sup>	
						Daeyeon	Seomyun
5/11	17:00-18:30	23.4	78.8	0.6	98.4	63**	52**
5/16	17:00-18:30	19.4	59.8	1.4	99.6	31	N/A
5/23	17:00-18:30	23.8	74.8	2.2	230.1	33	N/A
5/26	17:00-18:30	19.2	61.5	2.3	157.3	19	16
7/27	5:00-6:30	23.2	69.5	1.2	19.8	22	13*
	7:30-9:00	25.7		1.6	82.7	17	15*
	14:00-15:30	27.2		2.2	96.4	22	17
	17:00-18:30	27.3		1.4	100.6	18	16
8/1	5:00-6:30	25.9	79.6	1.3	30	20	25
	7:30-9:00	27.6		1.5	73.7	25	40**
	14:00-15:30	28.9		2.1	94.6	30	35**
	17:00-18:30	27.8		3	79	23	33

\* Good in terms of PM<sub>2.5</sub> (< 15 μg/m<sup>3</sup>)\*\* Bad in terms of PM<sub>2.5</sub> (> 35 μg/m<sup>3</sup>)

# Ambient concentrations obtained from Air Quality Monitoring Station

### 2.3. Temporal distribution according to transportation types

The time-series change of PM<sub>2.5</sub> concentration during the measurement period is shown in Fig. 2.3. The time-series change showed a significant difference in PM<sub>2.5</sub> concentration depending on transportation or location (Fig. 2.3), and this difference also showed a different pattern depending on the measurement time. For example, in May, the concentration difference was not large between the concentration in the bus and the concentration in walking, but in August, when walking compared to other transportation, the concentration sharply increased and decreased for a short period of time compared (Red line in Fig. 2.3).

This seems to have been affected by some of the effects of high-emission vehicles (high emitters) compared to other vehicles and by roadside smoking (ME, 2016; Choi et al., 2013). The amount of particulate pollutants emitted from a vehicle is concentrated at a very small size of 10 - 80 nm (Choi and Kim, 2018) and the number of particles emitted from a high-emission vehicle may be more than 20 times higher than that of a normal vehicle (Morawska et al., 2008). However, the effect on the mass concentration is relatively small due to the condensation particles of vehicle emission are very small compared to the accumulation mode particle size (Kumar et al., 2010). In observations, these spikes were not frequently observed (not here presenting results). This is attributed to the local impact of smoking or restaurant emissions in sidewalk rather than the impact of high-emission vehicles (NIER, 2019; ME, 2016). In fact, the spike in the number of particles strongly affected by vehicle

emissions is 10 times larger than the surrounding concentration, while the PM<sub>2.5</sub> spike is limited to 2–3 times the size of the surrounding concentration (Fig. 2.3).

PKNU (DY) was composed of a large area with no major emission source and low building density, so it showed lower concentration than the route from SM or DY subway station to PKNU (Fig. 2.3). SM has a lot of traffic on 8 lanes and smokers all over the road, so it has a lot of spikes and concentrations up to 18  $\mu\text{g}/\text{m}^3$  higher than DY (Fig. 2.3). The effect of tobacco smoke can be confirmed when spike appears in Figure 2.3, and the concentration increased to about 30 - 90  $\mu\text{g}/\text{m}^3$ , but since it disappears within 5 - 10 seconds. The difference between the amount of intake including spikes and without spikes was few if it doesn't stay a long time on a road or smoking area. But, the concentrations number of particles may increase from 10 to 100 times in near high emission sources, so the difference in exposure may increase (Choi et al., 2018; Goel and Kumar, 2015).

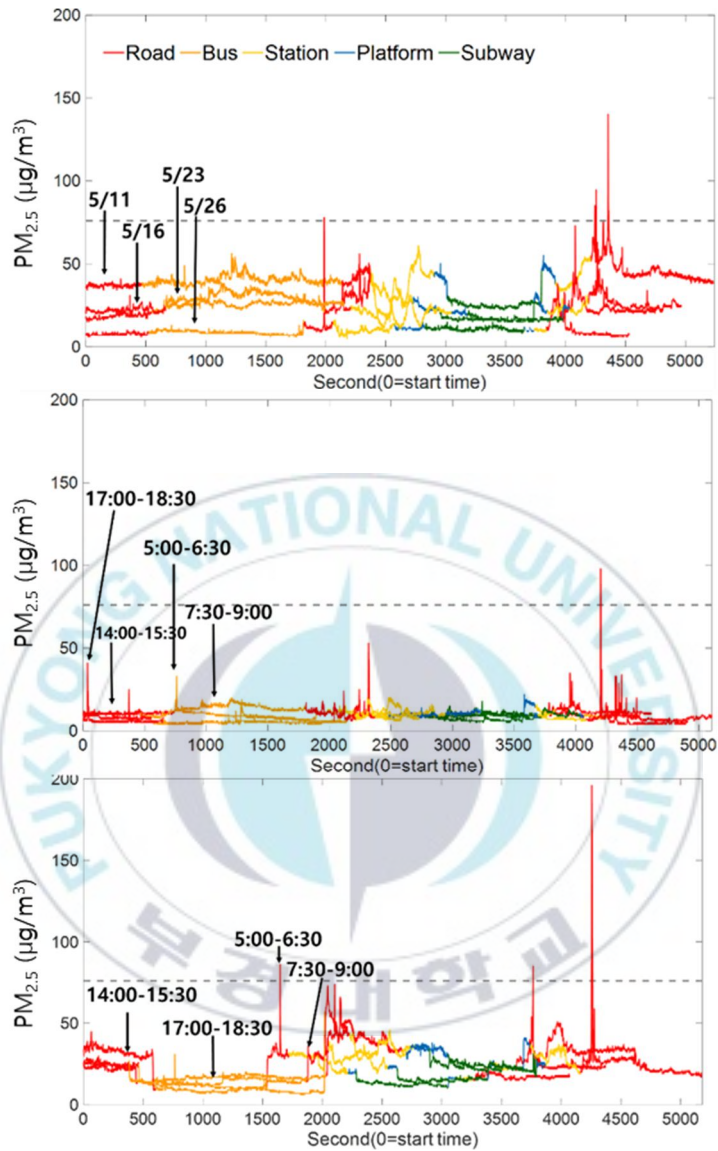


**Fig. 2.3** Time-series of  $PM_{2.5}$  concentrations for sampling periods. Red lines represent the walk along roadside, orange lines in-cabin of buses, yellow lines underground subway station, blue lines platform, and green lines in-cabin of subway train. X-axis is time in seconds with the departure = 0 s. (a) Time-series obtained in May of 2017 (17:00–18:30 LT). (b) and (c) show time-series for four different periods of a day on July 27 and August 1 of 2017, respectively. Gray horizontal lines represent the upper limits for good (solid), normal (dotted), and bad (dashed)  $PM_{2.5}$  conditions.

## 2.4. Difference in concentration by transportation types

If the concentration of PM<sub>2.5</sub> when walking is representative of the concentration of air in near the road, the concentration in the subway and bus generally show a positive correlation with atmospheric concentration. So, the concentration inside the subway and bus was affected by PM<sub>2.5</sub> concentration in the atmosphere (Fig. 2.4a). However, the effect of PM<sub>2.5</sub> concentration on the subway and bus was different. The concentration inside the subway showed 63% of PM<sub>2.5</sub> concentration in the outside atmosphere (Fig. 2.4a; slope = 0.67), which seems to be the factor determining the concentration in the subway cabin ( $R^2 = 0.91$ ).

The concentration inside the bus was divided into two cases. Buses without air conditioner (A/C) operation did not differ from the outside concentration or showed a tendency to be slightly higher, indicating that they were likely affected by emission in road (Fig. 2.4a; slope = 1.01). However, when air conditioner was operated on the bus (closed window) showed a tendency to maintain 5 - 15  $\mu\text{g}/\text{m}^3$  regardless of atmospheric concentration (shaded part in Fig. 2.4a). This is since the windows were closed, limited the inflow of PM<sub>2.5</sub> concentration, and circulating internal air, which led to the removal of PM<sub>2.5</sub> through air conditioner filters. Lee et al. (2014) suggested that when the air conditioner was operated in the internal circulation mode, the concentration of particulate matter inside the vehicle drastically decreased through a filter. This means that when the air conditioner is operated, the effect of the outflow of cold air inside the vehicle may be stronger than the inflow of

external air when the door is opened. Also, mixing with external air is not efficient while the car door is open. It is possible that it was not suitable to detect the effect directly due to measurement position on the bus. So, additional observations through more detailed experimental designs are needed to determine causes.

Through analysis of differences in measured concentrations for each transportation, when a high-density PM<sub>2.5</sub> event occurs, to minimize the exposure method is using an air-conditioned bus or vehicle in an air circulation mode rather than the subway.

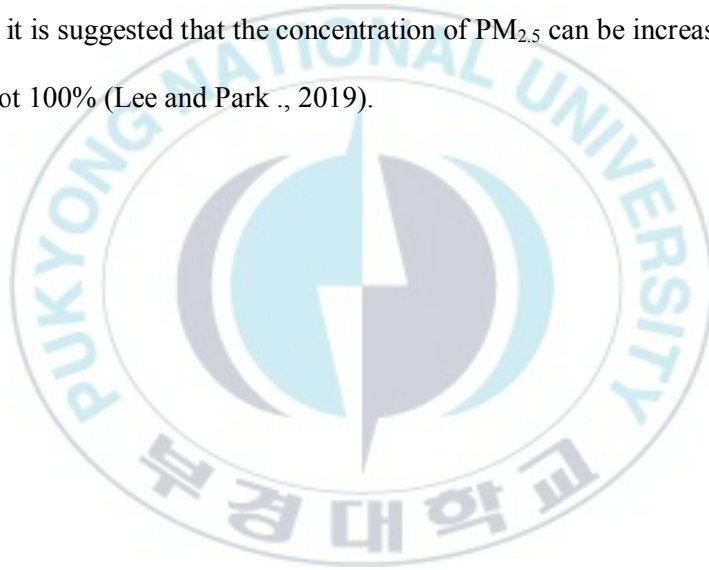
When using the subway, it goes through various environments within the station (underground station, subway station, inside the subway cabin). The concentration of PM<sub>2.5</sub> may vary depending on the location of the subway station. In subway stations in Seoul, it was suggested that the concentration inside the subway cabin (115.0 µg/m<sup>3</sup>) was higher than at the platform (105.0 µg/m<sup>3</sup>) (Park and Ha, 2008). However, subway line 2 in Busan, which is the subject of this study, the concentration inside the subway cabin is the lowest (Avg. 15.0 µg/m<sup>3</sup>), and then follows the underground station (Avg. 19.0 µg/m<sup>3</sup>), platform (Avg. 20.4 µg/m<sup>3</sup>). Compared to the external concentration, the platform showed 79% of the external concentration, underground station showed 83%, and the subway cabin showed 63% (Fig. 2.4b).

In all three sections of the subway, when the external concentration was 20 µg/m<sup>3</sup> or less, there was a small difference within the range of 0 - 5 µg/m<sup>3</sup>, but the higher the external concentration, concentration difference gradually increased. In addition, it showed a positive correlation with the outside concentration in all sites,



indicating that all sites of the subway, including inside the subway cabin, were strongly affected by the  $PM_{2.5}$  concentration outside (Fig. 2.4b;  $R^2 = 0.76 - 0.91$ ).

However, recent study, Lee and Park (2019) were measured in subway (station, platform, cabin) in Seoul, and showed high concentrations in the order of platform ( $100.2 \mu\text{g}/\text{m}^3$ ), station ( $73.6 \mu\text{g}/\text{m}^3$ ), and Outside ( $35.5 \mu\text{g}/\text{m}^3$ ). One of the reasons for its high concentration is It may be occurred pollution sources by trains such as tunnels. But, since  $PM_{2.5}$  control is performed inside the basement by ventilation, it is suggested that the concentration of  $PM_{2.5}$  can be increased when the control is not 100% (Lee and Park ., 2019).





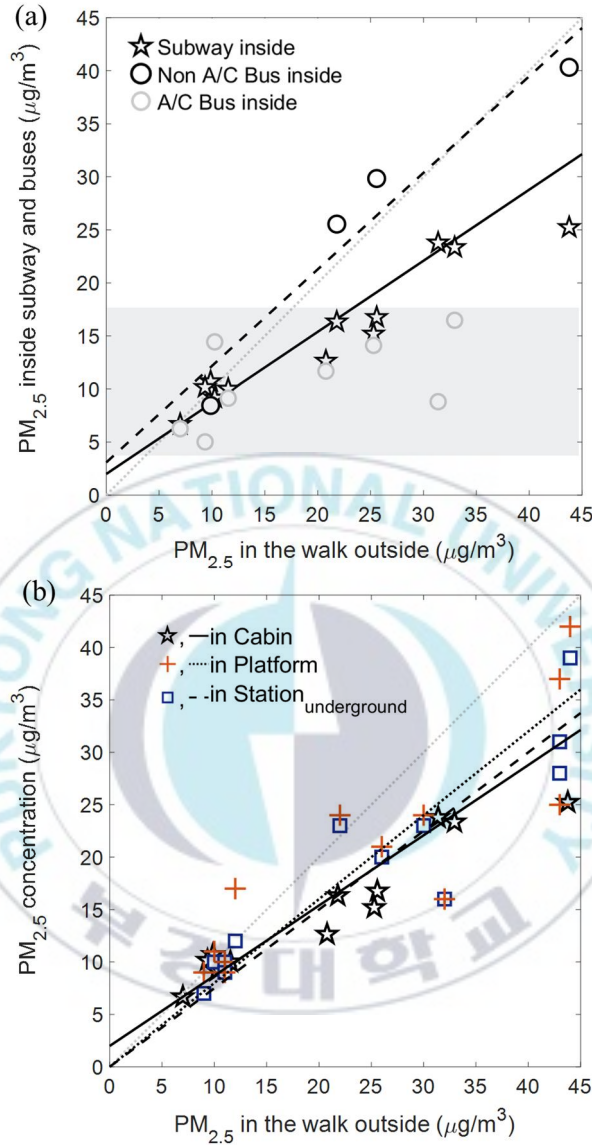


**Fig. 2.4** (a) Comparison plot of PM<sub>2.5</sub> levels measured between inside the transportation vs. walk outside. Stars indicate the PM<sub>2.5</sub> levels inside the subway, Black circles inside the A/C non-operated buses, and gray circles inside the A/C operated buses. Black solid line shows the linear fit for the inside subway (R<sup>2</sup> = 0.92), dashed line for A/C non-operated buses (R<sup>2</sup> = 0.91). (b) 1:1 plots of PM<sub>2.5</sub> concentrations between specific locations of subway and ambient outside. In-cabin of the subway train (R<sup>2</sup> = 0.91), at the platform (R<sup>2</sup> = 0.76), station (underground, R<sup>2</sup> = 0.85).

## 2.5. Inhalation rate according to ventilation rate

The PM<sub>2.5</sub> inhalation amount for each transportation was estimated by PM<sub>2.5</sub> mass concentration and the respiratory rate for each activity. Ventilation rate by activity used the measurement results of healthy adults of Fusi et al. (2005). It was assumed that the speed of an adult (male) walking slowly was 3.5 km/hr. The respiratory rate was used when standing outside and standing in a bus or subway. Volume of air inhaled per hour was calculated by using the volume of air inhaled in one breath (Tidal Volume, L/min) and ventilation rate per minute (Respiratory Rate, ash/min) (Eq. 2.1). Total PM<sub>2.5</sub> inhaled per unit time for each activity were calculated by using the volume of air inhaled per hour and measured PM<sub>2.5</sub> concentration (Eq. 2.2). Ventilation when standing was assumed to be  $9.7 \pm 2.2$  L/min and  $18.5 \pm 2.7$  L/min when walking (Fusi et al., 2005).

$$\begin{aligned} \text{Ventilation [L/min]} &= \text{Tidal volume [L/breath]} \\ &\times \text{Respiratory rate [breaths/min]} \quad (\text{Eq. 2.1}) \end{aligned}$$

$$\begin{aligned} \text{Inhalation rate } [\mu\text{g/min}] &= \text{Ventilaton [L/min]} \times \\ &\times \text{PM}_{2.5} [\mu\text{g/m}^3] \times 0.001 [\text{m}^3/\text{L}] \quad (\text{Eq. 2.2}) \end{aligned}$$

For the entire measurement period, the highest inhalation rates ( $0.38 \pm 0.21$   $\mu\text{g/min}$ ) when walking from outsides. When using the bus ( $0.15 \pm 0.10$   $\mu\text{g/min}$ ) and when using the subway ( $0.14 \pm 0.06$   $\mu\text{g/min}$ ) showed inhalation rates of 40% and 37%

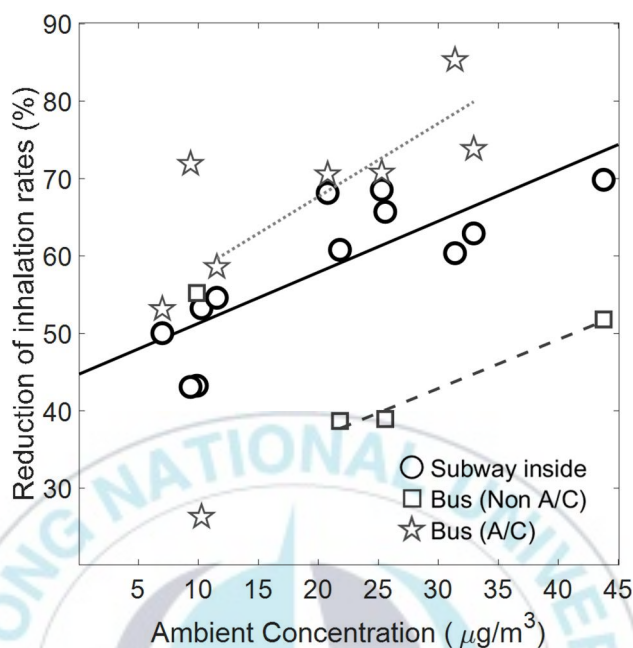
of inhalation rates when walking, respectively. Especially on May 11, during the high concentration PM<sub>2.5</sub> events, the inhalation rates was high in order, walking ( $0.81 \pm 0.14 \mu\text{g}/\text{min}$ ), bus ( $0.39 \pm 0.03 \mu\text{g}/\text{min}$ ), subway ( $0.24 \pm 0.01 \mu\text{g}/\text{min}$ ). The inhalation rates of inside buses and subways were 48% and 30% of walking, respectively. This is because the external concentration was higher than that of the bus or subway and increased ventilation rate when walking (Table 2.3).

Figure 2.5 shows the reduced inhalation rates when using the subway or bus compared to inhalation rates of walking according to the external PM<sub>2.5</sub> concentration. When the external concentration is low ( $< 15 \mu\text{g}/\text{m}^3$ ), since the concentration in the bus or subway is small, the reduction rate in PM<sub>2.5</sub> inhalation rates per minute is around  $0.1 \mu\text{g}$  (Fig. 2.5). This decrease was largely due to differences in ventilation rates. However, as the ambient PM<sub>2.5</sub> concentration increases, the effect of reducing the inhalation rates gradually increases (A/C operated bus: slope  $-0.016 >$  subway: slope  $-0.013 >$  A/C non-operated bus: slope  $-0.010$ ) (Fig. 2.5).

The result indicates that the higher the concentration of PM<sub>2.5</sub>, to reduce the exposure of PM<sub>2.5</sub> the less external activity possible and using the subway. In particular, the exposure time decreases when using the subway rather than walking. It is shown that the total exposure during movement ( $= \text{inhalation rates} \times \text{exposure time}$ ) can be further reduced.

**Table 2.3** Inhalation rates ( $\mu\text{g}/\text{m}^3$ ) estimated for the in-cabin of the subway and buses, and the walk outside for the sampling periods.

Date	Sampling time	Subway inside (std)	Bus inside (std)	Walk (std)
5/11	17:00-18:30	0.24 (0.01)	0.39 (0.02)	0.81 (0.14)
5/16	17:00-18:30	0.16 (0.01)	0.29 (0.02)	0.47 (0.09)
5/23	17:00-18:30	0.15 (0)	0.25 (0.01)	0.4 (0.08)
5/26	17:00-18:30	0.10 (0.01)	0.08 (0.01)	0.18 (0.09)
7/27	5:00-6:30	0.09 (0)	0.14 (0.02)	0.19 (0.02)
	7:30-9:00	0.10 (0.01)	0.09 (0.02)	0.21 (0.06)
	14:00-15:30	0.10 (0.01)	0.05 (0)	0.17 (0.05)
	17:00-18:30	0.06 (0)	0.06 (0.01)	0.13 (0.05)
8/1	5:00-6:30	0.12 (0.01)	0.11 (0.01)	0.38 (0.10)
	7:30-9:00	0.14 (0)	0.14 (0.02)	0.47 (0.08)
	14:00-15:30	0.23 (0.02)	0.09 (0.03)	0.58 (0.22)
	17:00-18:30	0.23 (0.01)	0.16 (0.02)	0.61 (0.14)
Average		0.14 (0.06)	0.15 (0.10)	0.38 (0.21)



**Fig. 2.5** Decreases in inhaled  $\text{PM}_{2.5}$  in the cabin of subways and buses as a function of ambient  $\text{PM}_{2.5}$  levels. Inhalation rates of  $\text{PM}_{2.5}$  in the cabin ( $[\text{InhalR}]_{\text{cabin}}$ ) over the rates of the walk along the roadside ( $[\text{InhalR}]_{\text{walk}}$ ). ( $[\text{Inhalation rates in cabin}] - [\text{Inhalation rates in walk}]$ ): fitting equations are  $-0.016 \times [\text{PM}_{2.5}] + 0.06$  for A/C operated buses (grey dotted line);  $-0.013 \times [\text{PM}_{2.5}] + 0.04$  for subway (black solid line);  $-0.010 \times [\text{PM}_{2.5}] + 0.03$  for A/C non-operated buses (gray dashed line).

## 2.6. Summary

PM<sub>2.5</sub> concentration and inhalation rates were quantified by public transportation (bus, subway) and walking. PM<sub>2.5</sub> concentration according to the surrounding environment was the highest in the A/C unoperated bus (27.1 µg/m<sup>3</sup>), walking on the road (24.4 µg/m<sup>3</sup>), subway platform (20.4 µg/m<sup>3</sup>) and walking on the university main entrance (19.9 µg/m<sup>3</sup>), in subway (15.0 µg/m<sup>3</sup>), and in A/C operation bus (10.2 µg/m<sup>3</sup>).

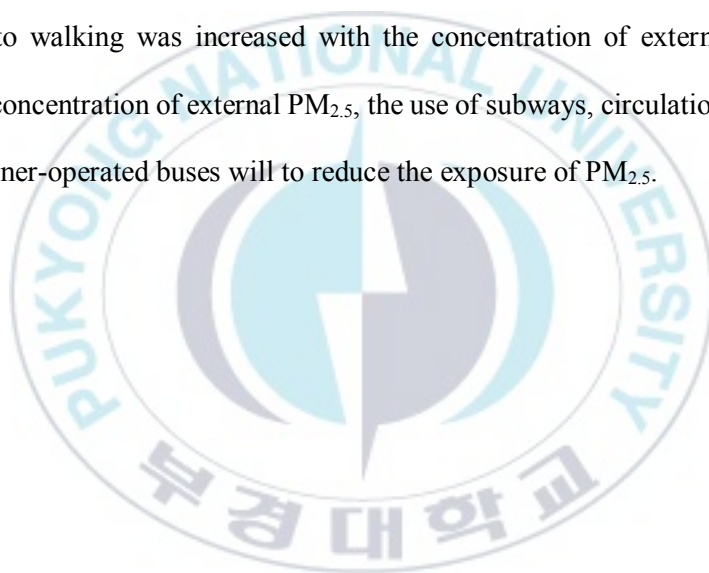
The concentration of the subway and the bus showed a very good correlation with the external concentration ( $R^2 = 0.88$  and  $0.92$ , respectively). The concentration inside the public transportation was strongly affected by the external PM<sub>2.5</sub> concentration. However, the concentration of the A/C operation inside bus remained within 20 µg/m<sup>3</sup> regardless of the external concentration. When the external concentration is high, closing the window of the bus and using the air conditioner in the circulation mode are the most efficient ways to reduce the exposure.

In subway, the concentration difference was shown in the order of platform (20.4 µg/m<sup>3</sup>), subway station underground station (19.0 µg/m<sup>3</sup>), and subway cabin (15.0 µg/m<sup>3</sup>), which was 83%, 79% and 63%, respectively.

The concentration of PM<sub>2.5</sub> in the platform has decreased by 44% since the installation of the screen door (Lee et al., 2009). However, it is impossible to determine the effect of the screen door because the concentration before the screen door installation cannot be confirmed. If the concentration of the platform was the

highest because the direct exchange between the platform and the external air, which is the deepest place of the subway station underground, installing a filter in the ventilation could be a way to reduce both the concentration of the platform and the inside of the subway vehicle.

The  $PM_{2.5}$  inhalation rates according to the ventilation rate by transportation was 48% (bus) and 30% (subway) compared to the walking distance from the roadside. Also, the decrease of  $PM_{2.5}$  inhalation rates when using buses and subways compared to walking was increased with the concentration of external  $PM_{2.5}$ . In higher the concentration of external  $PM_{2.5}$ , the use of subways, circulation modes and air conditioner-operated buses will to reduce the exposure of  $PM_{2.5}$ .





## CHAPTER 3

### A HIGHLY DENSE COST-EFFECTIVE SENSOR NETWORK

#### 3.1. Monitoring site

The monitoring site have a road network with heavy traffic in site, include large buildings and low buildings, and opening space, as well as the air quality monitoring station (AQMS) and the Korea Meteorological Administration Automatic Weather Station (AWS) within the 2 km by 2 km range. So, data was obtained from reference equipment (Fig. 3.1). Because the main purpose is to look at the detailed pollution distribution in the city center, construction sites or complex pollutants are excluded from observation points, and sensor networks are divided into four main roads according to the characteristics of land-use within observation points: (1) Site 1 (Eulji-ro); (2) Site 2 (Sogong-ro); and (3) Deoksugung-gil, which includes large buildings and low buildings or vacant lots, started from the City Hall Square; (4) Site 4 (Namdaemun-ro) (Table 3.1) Sensor nodes were installed on lamppost at ~ 2.5 m height above the ground in roadsides. We installed sensor nodes in a pair facing each other in the roadside. We also attempted to see the vertical distributions of air pollutants, placing two sensor nodes on the roofs of the tallest building in the urban street site (132 m AGL; Site 1) and the attached fourth-floor building (14 m AGL).



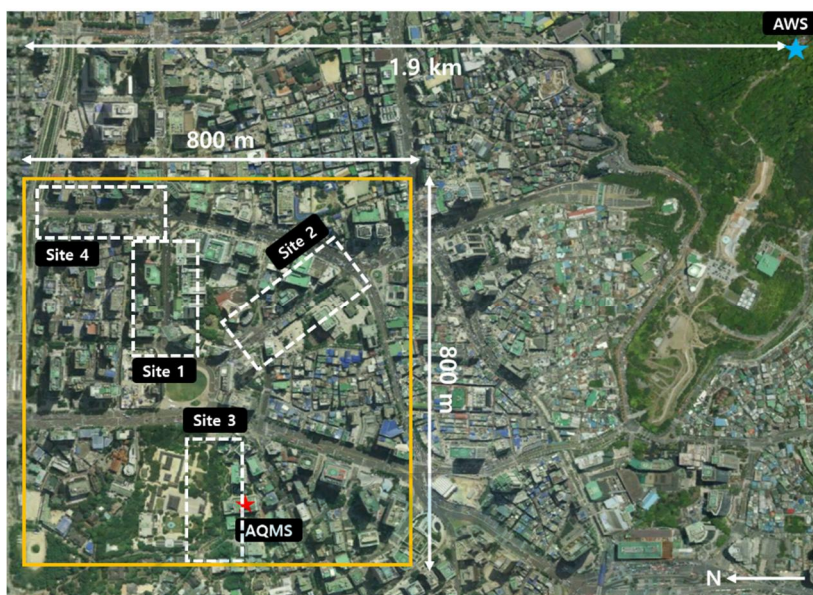


**Fig. 3.1** Satellite image for the monitoring domain including spatial scales of the domain. The yellow box indicates the observation site in the 800 m  $\times$  800 m in Seoul. The red star represents the Air Quality Monitoring Station (AQMS), and the blue star represents the Automatic Weather Station (AWS) location within 2 km in the observation site. (1) Site 1 (Eulji-ro); (2) Site 2 (Sogong-ro); (3) Site 3 (Deoksugung-gil) (4) Site 4 (Namdaemun-ro).



**Fig. 3.2** Image of the sensor assembly.

**Table 3.1** Each road characteristic and observation period.

Qualitative characteristic	Site1	Site2	Site3	Site4
Surroundings	Typical urban canyon	Large open lot and low buildings	Pedestrian-oriented one lane road.	It is composed of large buildings on both sides of the road, but the space between the buildings is large and low buildings and vacant lands exist.
Building Composition	surrounded by tall buildings on both sides of the road	buildings between several large buildings	Medium sized building on one side and empty lot on the other	
Road width	~ 21 m	~ 13 m	~ 3.5 m	~ 28 m
Traffic	Medium traffic with traffic predominantly in the direction of the city hall. Many public transportation vehicles such as buses and taxis.	Due to the narrow roads, the traffic volume is not much higher than that of Site1, but it is particularly heavy during the day.	Vehicle control from 11:00 to 13:00. At other times, traffic is minimal compared to the surroundings through pedestrian-oriented one-lane roads.	There is a lot of traffic in both directions, but due to wide roads, traffic jams are not so severe.
Average building height around road	64 m	45 m	22.5 m	31 m
Setback distance from boundary line	both sides wide	both sides narrow	narrow	one sides wide
Sensor installation height	3.5 m	~ 2.5 m	~ 2.5 m	~ 2.5 m
Higher stories				
Sensor Installation	14 m / 132 m	N/A	N/A	N/A
Observation period	Summer : 2017.8.25 00:00 -9.1 00:00 Winter : 2018.1.9 00:00 -23 00:00			Winter : 2018.1.9 00:00 - 23 00:00

Each sensor node consists of O<sub>3</sub>, NO<sub>2</sub>, CO, PM<sub>2.5</sub> and PM<sub>10</sub>, temperature, humidity sensor and Fan (ventilation rate: > 20 times / 1 minute). Table 3.2 provides platform information for gas and particle sensors respectively. Further details on the assessment of the characteristics and performance of the sensor nodes are covered by Park et al (2020). The sensor node stores data at a 10-second interval on the SD card, and communicates with the smartphone via wifi to display the states of sensors, pollutant concentrations, and battery levels. We used a lead-acid battery for the power of the sensor node to avoid the risk of explosion and the battery was periodically replaced.






To compare air quality among a large number of sensor nodes located in various urban microenvironments, the consistency of readings among a large number of nodes should be quantitatively evaluated. In this respect, we conducted intercomparison tests placing 30 sensor nodes at the same place (Pukyong National University campus) for 2 - 4 days before and after air quality monitoring experiments. The intercomparison tests were performed in real atmospheric conditions. The readings from all sensor nodes showed great consistency ( $R^2 > 0.74$ ) and the relationships of sensor readings between sensor nodes did not change before and after the monitoring experiments. Based on intercomparing results, we corrected sensor readings from 29 sensor nodes corresponding to those of the reference sensor node (1st step correction, Table 3.3).

For the monitoring experiment periods, we placed the reference sensor node in close proximity to the inlet of AQMS (located 2 km east from the monitoring site) to

conduct intercomparing test between the sensor node and FRM (Federal Reference Method)/FEM (Federal Equivalent Method) instruments. For all air pollutants (except NO<sub>2</sub>), the sensor node showed good consistency with FRM/FEM instruments for both the summer and winter experiment periods ( $R^2 > 0.80$ ; Fig. 3.3). Thus, based on these intercomparing results, we corrected all 29 sensor nodes data, which was initially corrected corresponding to those of the reference sensor readings, were secondly corrected corresponding to officially valid concentrations of FRM/FEM instruments (2nd step correction, Fig. 3.3). NO<sub>2</sub> sensors appeared to be sensitive to weather conditions and potential interferences (e.g., O<sub>3</sub>) and showed seasonal discrepancies with FRM/FEM instruments (Park et al., 2020; Mead et al., 2013). Thus, we additionally corrected NO<sub>2</sub> sensor readings with multi-variate regression method using O<sub>3</sub>, temperature, and humidity as explanatory variables (3rd step correction, Fig. 3.3c, d).

The finally corrected air pollutant concentrations from the sensor nodes agreed well with those of the FRM/FEM instruments. We also compared corrected air pollutants concentrations from the sensor node to those of FRM/FEM instruments at nearby AQMS located within the monitoring site, and found good consistency between two dataset considering the sensor node and AQMS were apart ~ 40 m horizontally and ~ 17.5 m vertically (2.5 m AGL for sensor node vs. ~ 20 m AGL for AQMS inlet) (Fig. 3.1). More details about the correction processes for sensor node readings are found in Park et al. (2020)

**Table 3.2** Sensor specifications.

Type	Sensor	specifications
CO	 Alphasense CO-B4	<ul style="list-style-type: none"> <li>• Linearity test with reference method: <math>R^2=0.88</math>, slope=0.94 (5min.avg.)</li> <li>• Noise level : 4 ppb</li> <li>• Range: up to 1000 ppm</li> <li>• Operating conditions: -30~50 °C / 15~90% RH</li> <li>• Reference: Cross et al. (2017)</li> </ul>
NO <sub>2</sub>	 SGX MiCS-2710	<ul style="list-style-type: none"> <li>• Detection limit: 11.6 ppb</li> <li>• Linearity test with reference method: <math>R^2=0.98</math></li> <li>• Accuracy: 3 ppb</li> <li>• Operating conditions: -30~85 °C / 5~95% RH</li> <li>• Response time: &lt; 1 min.</li> </ul>
O <sub>3</sub>	 Aeroqual SM50	<ul style="list-style-type: none"> <li>• Linearity test with reference method: <math>R^2=0.91\sim0.97</math>(Jiao et al., 2016)</li> <li>• Calibrated range: 0 – 150 ppb</li> <li>• Accuracy: &lt; 10 ppb</li> <li>• Resolution: 1 ppb</li> <li>• Operating conditions: -20~50 °C / 5~95% RH</li> </ul>
PM <sub>2.5</sub> /PM <sub>10</sub>	 Plantower PMS3003	<ul style="list-style-type: none"> <li>• Linearity test with reference method: <math>R^2=0.92</math>, slope=0.97 (1hour avg.)</li> <li>• Range of concentrations: 0~500 <math>\mu\text{g m}^{-3}</math></li> <li>• Resolution : 1 <math>\mu\text{g m}^{-3}</math></li> <li>• Operating conditions: -10~60 °C / 0~99% RH</li> <li>• Counting efficiency : 50% at 0.3 <math>\mu\text{m}</math> and 98% at <math>\geq 0.5 \mu\text{m}</math></li> </ul>
Temp./Humid.	 Sensirion SHT21	<ul style="list-style-type: none"> <li>• Resolution: 0.01 °C / 0.04%</li> <li>• Accuracy: <math>\pm 0.3</math> °C / <math>\pm 2\%</math></li> <li>• Operating conditions: -40~125 °C / 0~100%</li> <li>• Based on manufacturer specification document</li> </ul>
Data logger	Atmel/ATmega2560	<ul style="list-style-type: none"> <li>• Digital I/O Pins: 54 (of which 15 provide PWM output)</li> <li>• Analog Input Pins: 16bit,</li> <li>• Clock Speed: 16 MHz</li> <li>• Micro SD memory: 16GB</li> <li>• RTC : Rechargeable Battery (5.8mAh), 30day</li> </ul>



**Table 3.3** Results of linear regression between 29 sensors and the reference sensor in summer and winter (using 15-minute averaged unadjusted data). The reference sensor represents the sensor node that was co-located with FRM/FEM instruments at AQMS (Park et al., 2020).

Summer (Aug. and Sep.)		CO	NO <sub>2</sub>	O <sub>3</sub>	PM <sub>2.5</sub>	PM <sub>10</sub>
Slope	Mean	0.87	1.03	1.00	0.94	0.93
	(std)	(0.08)	(0.08)	(0.04)	(0.04)	(0.04)
	Range	0.74–1.13	0.88–1.23	0.96–1.06	0.87–1.01	0.85–1.00
R <sup>2</sup>	Mean	0.940	0.982	0.997	0.945	0.933
	(std)	(0.055)	(0.012)	(0.001)	(0.012)	(0.012)
	Range	0.739–0.979	0.953–0.997	0.994–0.998	0.911–0.964	0.905–0.951
# of data (N)		312	284	325	342	342
Winter (Dec. and Jan.)		CO	NO <sub>2</sub>	O <sub>3</sub>	PM <sub>2.5</sub>	PM <sub>10</sub>
Slope	Mean	0.90	1.17	0.96	1.03	1.01
	(std)	(0.06)	(0.30)	(0.06)	(0.06)	(0.07)
	Range	0.79–1.07	0.83–1.66	0.87–1.05	0.84–1.12	0.80–1.12
R <sup>2</sup>	Mean	0.972	0.965	0.975	0.991	0.988
	(std)	(0.039)	(0.020)	(0.004)	(0.008)	(0.006)
	Range	0.960–0.988	0.934–0.994	0.970–0.981	0.955–0.995	0.961–0.993
# of data (N)		484	377	463	574	574

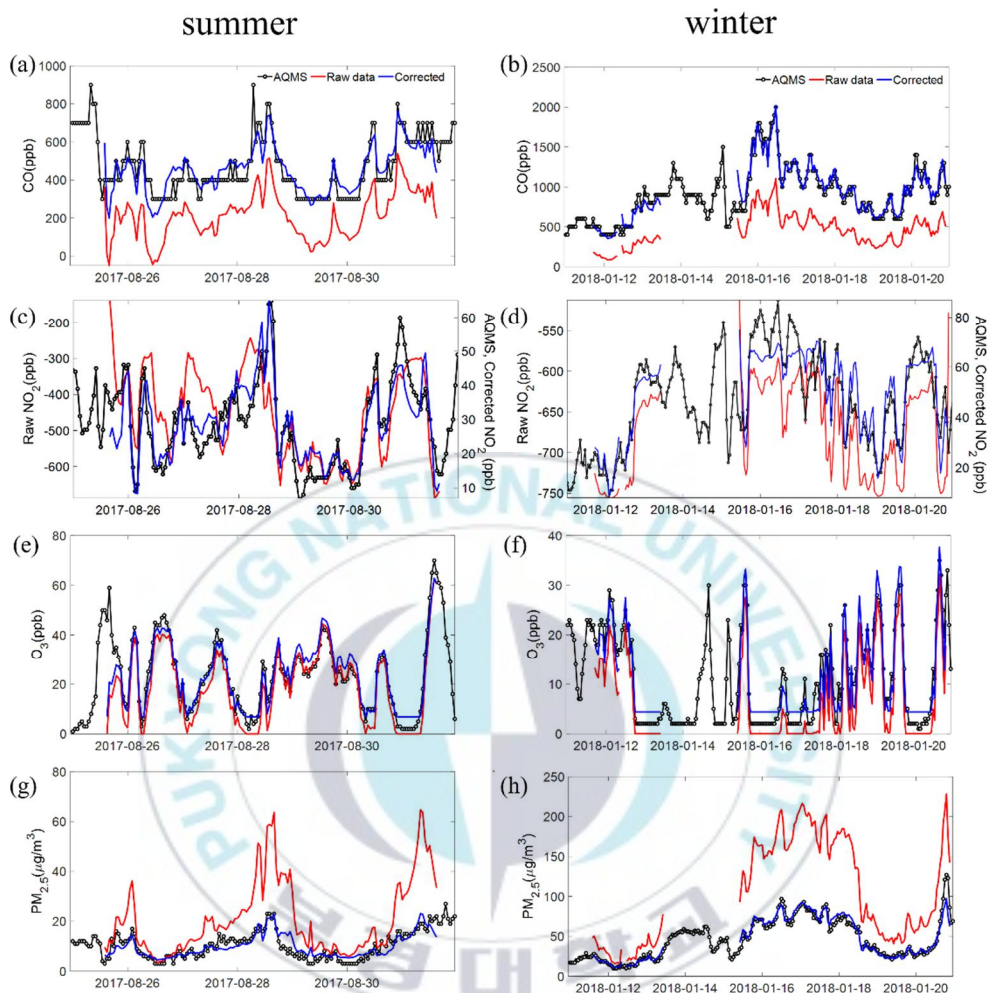


**Fig. 3.3** Results of the comparison between AQMS and unadjusted sensor data for summer and winter (hourly averaged data): in summer (a) CO, (c) NO<sub>2</sub>, (e) O<sub>3</sub>, (g) PM<sub>2.5</sub>; in winter (b) CO, (d) NO<sub>2</sub>, (f) O<sub>3</sub>, (h) PM<sub>2.5</sub>. Red line represents raw data and blue line indicate corrected data. The black dotted lines denote AQMS data.



## 3.2. Meteorological conditions

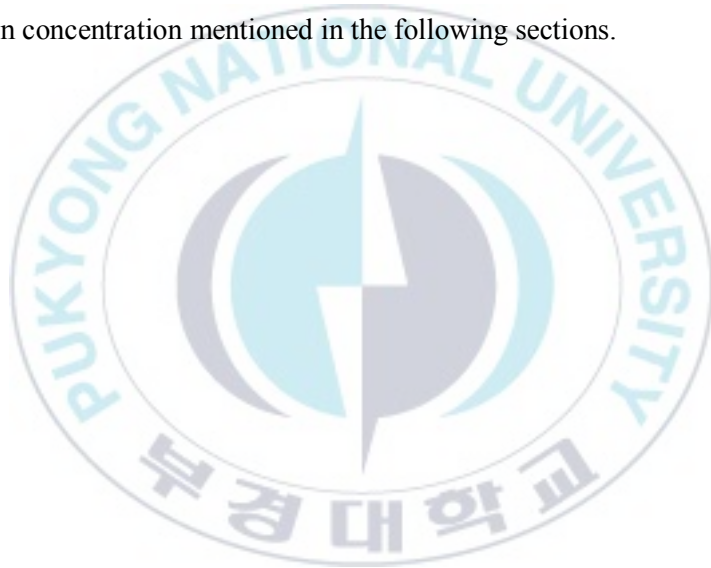
Weather data were provided by the Korea Meteorological Administration (KMA, Automatic Weather System) located within 2 km of the monitoring site (Fig. 3.1). During summer observations rainfall occurred intermittently once or twice during the observation period, with significant rainfall occurring two days before observations began (August 23). The average temperature of the upper AWS was 15.2 to 30.6 ° C (average  $21.2 \pm 3.3$  ° C), and the average wind speed was  $2.0 \pm 1.2$  m/s (6.3 m/s maximum wind speed). The average wind speed in the ground AWS (in Site 1) was  $0.9 \pm 0.7$  m/s (about 1.8 m AGL), which was about 45% lower than the upper wind speed. The maximum wind speed on the ground was 3.62 m/s (wind direction: north), at which time the upper layer was 2.9 m/s (wind direction: west), about 0.8 times stronger than the upper layer (Fig. 3.4 a, Table 3.4).

Strong cold and snow events occurred the day before the winter observation (January 8), and heavy snow/storms occurred on the afternoon of the last observation day (January 22). The mean temperature of the upper layer (interval 5 minutes) was -16.2 to 7.4 ° C (average  $-3.2 \pm 6.6$  ° C). The upper mean wind velocity was  $2.4 \pm 1.4$  m/s (maximum wind velocity of 10.3 m/s) (Fig. 3.4b, Table 3.4). The average ground wind speed measured in the same time was recorded at  $1.0 \pm 1.2$  m/s, which was 42% lower than the upper wind speed (at Site 2, about 1.8 m AGL). When the maximum wind speed was blowing at the upper level, the ground wind speed was lower than

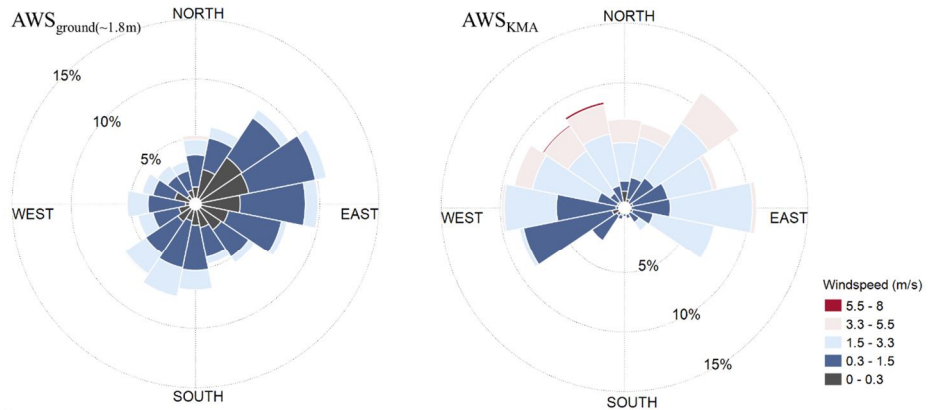
that of the upper floor (AWS, KMA 10.3 m/s vs. AWS 2.4 m/s) due to the blocking of buildings considering the direction of the road (northwest-south).

When comparing wind direction/wind speed in summer, the wind speed of the ground (Site 1) was similar than the upper wind speed (KMA, AWS) when the upper wind direction was blowing east-west, but the wind speed was much smaller in the other direction. When the wind direction of the upper wind direction was west, the wind speed on the ground was proportional to 90% of the wind speed of the main wind speed (KMA, AWS wind speed 1.28 m/s vs. ground wind speed 1.15 m/s). On the other hand, if the wind direction of the main wind is from the northeast wind, the wind speed on the ground was very weak at 35.6% of the wind speed of the main wind speed (KMA, AWS wind speed 1.56 m/s vs. ground wind speed 0.56 m/s) and the wind direction was not constant. In particular, if the wind direction was not specified, the wind speed on the ground was very weak within 10% of the main wind speed (KMA, AWS wind speed 1.74 m/s vs. the ground wind speed 0.17 m/s). This tendency is influenced by the main wind if the direction of Site 1 road coincides with the direction of the road in the east-west direction, but if the wind blows in the other direction, the wind speed is cut off in the building and the wind speed is considerably lowered. The main wind direction of the winter ground (Site 2) was recorded as northwest and north wind; if the wind direction was northwest, the wind direction of AWS (KMA) was mainly west wind (57%) and northwest wind (17%). Winds were blowing in the west (56%) and northwest (16%) if the wind direction was north. As in summer, if the direction of the road (Southern-Northwest) and the main wind direction were consistent, the ground wind speed was affected by the main wind speed.

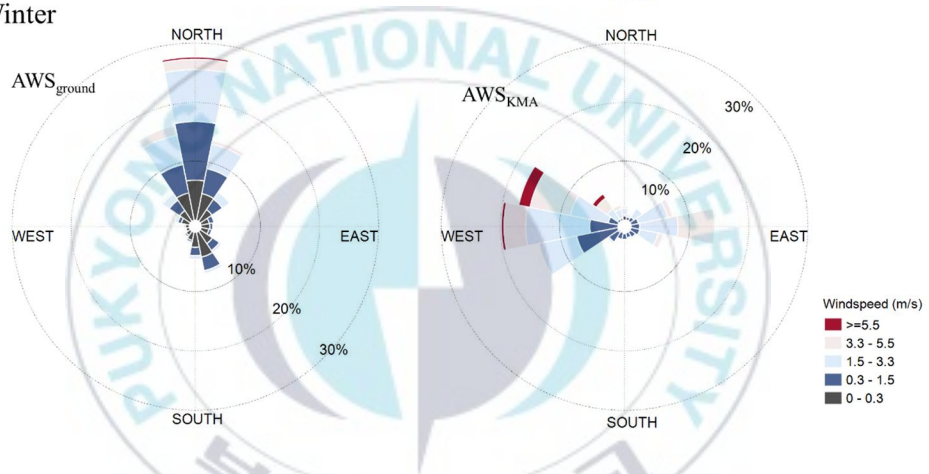
However, the wind direction was rarely consistent with the direction of the road (28 %) in winter. Regardless of the direction, the wind speed on the ground showed a low value even if a strong wind speed was blowing in the upper layer. When the wind was blowing from the east, it was very weak at 8% of the upper wind speed (KMA, AWS. 2.71 m/s. vs Ground 0.18 m/s). Therefore, it seems that relatively strong winds appear when blowing parallel to the direction of the urban canyon, regardless of summer or winter (Fig. 3.5). This difference in wind speed is likely to be one of the causes of the difference in concentration mentioned in the following sections.



(a) Summer



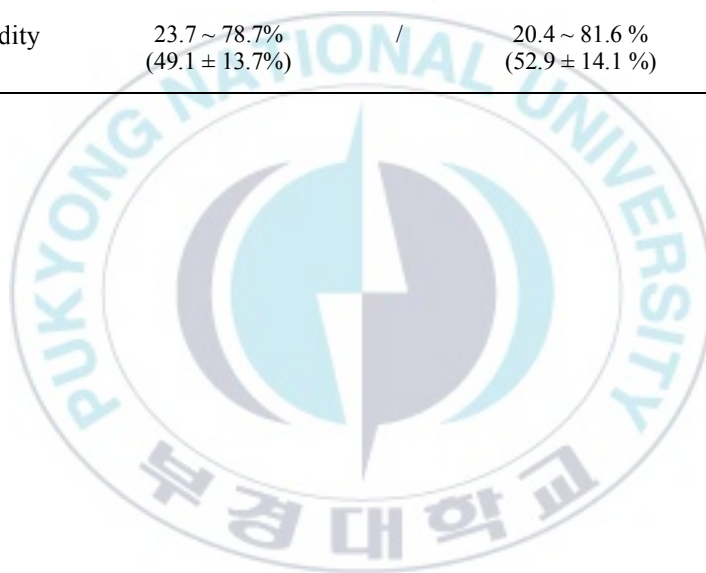
(b) Winter



**Fig. 3.4** The wind speed and wind direction of the ground and the upper layer (using 5min data). The wind speed range used the Beaufort wind force scale. The left panel is the ground AWS, the right panel is KMA, AWS. (a) Windrose in summer, (b) Windrose in winter.

**Table 3.4** Meteorological conditions.

	Summer		Winter	
	AWS <sub>ground(~1.8m)</sub>	AWS <sub>KMA</sub>	AWS <sub>ground(~1.8m)</sub>	AWS <sub>KMA</sub>
Calm (windspeed ≤ 0.3 m/s)	29 %	5.7 %	39 %	3.8 %
Temperature	18.4 ~ 30.5 °C (23.4 ± 3.2 °C)	15.2 ~ 30.6 °C (21.2 ± 3.3 °C)	-13.6 ~ 8.6 °C (-0.9 ± 6.4 °C)	-16.2 ~ 7.4 °C (-3.2 ± 6.6 °C)
Humidity	23.7 ~ 78.7% (49.1 ± 13.7%)	/	20.4 ~ 81.6 % (52.9 ± 14.1 %)	/



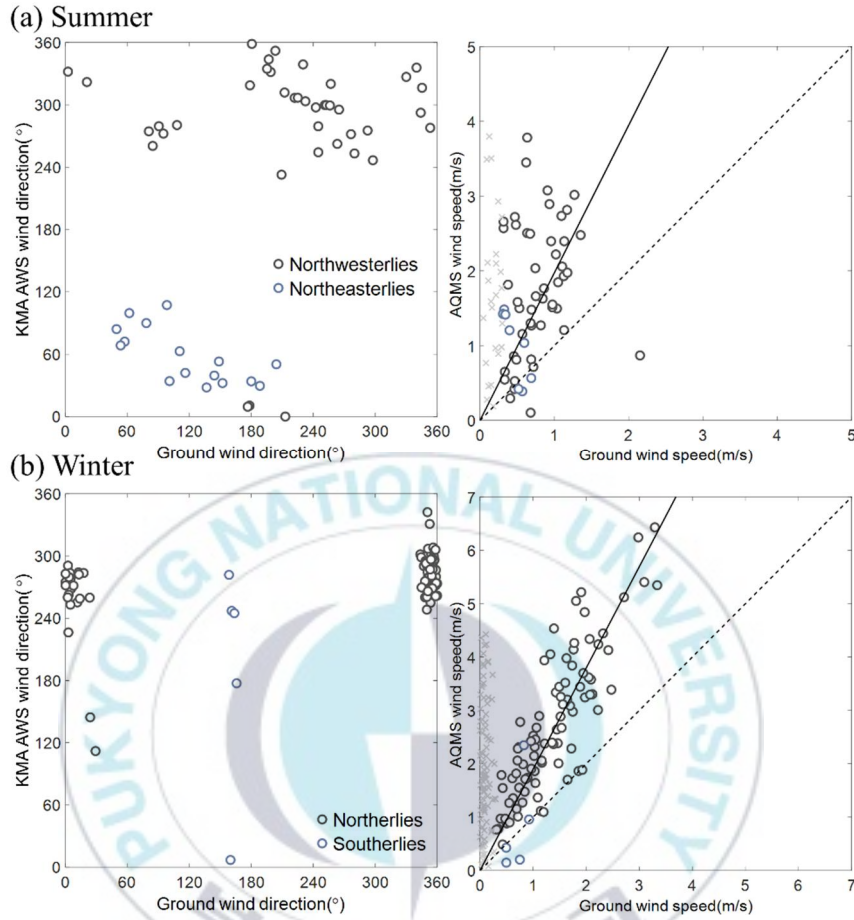


**Fig. 3.5** Wind direction/wind speed comparison of the upper layer (KMA, AWS) and the ground (summer: Site 1, winter: Site 2) in the vertical direction. The gray 'x' represents the case where the wind speed is weaker than 0.3 m/s and there is no wind direction. (a) In the summer, it was divided based on the wind direction of the upper wind direction. The black line represents the linear line ( $R^2 = 0.47$ ,  $ws_{KMA,AWS} = 1.8 ws_{ground}$ ) between the KMA, AWS wind speed and ground AWS when the upper wind is the main wind (Northeasterlies). (b) In winter, it was divided based on the wind direction of the ground. The black line represents the linear line ( $R^2 = 0.98$ ,  $ws_{KMA,AWS} = 1.9 ws_{ground}$ ) between the KMA, AWS wind speed and ground AWS when the main wind is on the ground (Northerlies).

### 3.3. Temporal distribution

The daily concentration distribution of four observation sections with different traffic volume and surrounding urban architecture environment was shown (Fig. 3.6). The four observation sections are approximately 100 to 400 m apart from each other, so the average concentration and concentration distribution of that section can represent different traffic and dry environments under the same local weather conditions. The overall daily variation was similar to that of AQMS in both summer and winter (Fig. 3.6). This suggests that the trend of temporal change in the unit of pollutants is mainly influenced by the characteristics of the synoptic meteorological and the local emission. In addition, the concentration was higher in winter than in summer, showing a typical seasonal tendency of primary pollutants. Because it is an environment that easy to accumulate under the atmospheric boundary layer and stable atmospheric conditions in winter, so most pollutants have a higher concentration in winter. High concentration events in winter were more pronounced  $PM_{2.5}$  (Fig. 3.6d). The concentration early in the winter observation period was recorded lower value as a result of accompanying by cold wave and snow and maintained lower value due to the less change during the day for all pollutants.

CO was a consistent difference in the concentration distribution for each site (Fig. 3.6a). In summer, Site 3 was recorded the lowest concentration distribution, Site 2 recorded the highest concentration distribution, and in the winter, it showed the lowest concentration in Site 3 as in summer and the high concentration distribution



in Site 2 and Site 4. This distribution is similar to the traffic volume and traffic congestion on each road. Therefore, the spatial distribution of CO concentration can be determined by the difference in CO emissions from the road and the distribution of the wind field at the same time. For example, in Site 2, the road lies in the northwest-southeast direction, and when the ground wind blows in a direction similar to the road direction, strong wind speed can increase the diffusion efficiency of pollutants and reduce the concentration in the atmosphere. Particularly, when this is consistent with the wind direction of upper and road direction, the efficiency of diffusion increases further (Fig. 3.7). However, in winter, the wind direction that consists of road direction of Site 2 was rare (28%). Also, the relatively small in-canopy volume by the road width was narrow and weak wind speed could decrease the diffusion efficiency and increase the concentration of pollutants.

The concentration distribution of NO<sub>2</sub> showed similar concentration in summer and early observation in winter. When higher PM<sub>2.5</sub> concentration events occurred, the concentration of NO<sub>2</sub> was higher, but it was not higher the increase rate than CO and PM<sub>2.5</sub>. Also, in summer, the difference of concentration was obvious for each site (Site 3 << Site 1 < Site 2), but this difference did not appear in high PM<sub>2.5</sub> concentration events. Concentration differences of the site recorded like summer at low concentration events, in winter although it was not as clear as in summer (Fig. 3.6b).

NO<sub>2</sub> and O<sub>3</sub> were inversely related to the difference in each site. That is, the concentration of O<sub>3</sub> was significantly lower in Site 1 and Site 2 than in Site 3, where NO<sub>2</sub> was relatively high in the summer. At Site 1 and Site 3, which had relatively low

concentration of  $\text{NO}_2$  in winter, recorded significantly higher ozone concentrations than Site 2 and Site 4. This is due to the chemical removal of ozone by  $\text{NO}_x$  emitted from the vehicle. In summer and early observation winter when the concentration of pollutants was low, concentration differences of  $\text{NO}_2$  showed a similar pattern to  $\text{CO}$ , it is that the concentration differences of the pollutants occurred by local traffic.

In the case of Site 2, the traffic volume is lower than other roads, but the road width is narrow, and the congestion is frequent. The difference in the concentration of Site 1 and Site 4 with similar traffic volume can be thought to be due to the influence of the weather field. The main wind direction of the upper in winter coincided with the road direction of Site 1, the diffusion of concentration was more effective than other areas, so pollutant concentration is low in spite of the high traffic volume (Fig. 3.8).

$\text{O}_3$  was not observed at night due to the characteristic of the sensor, so the data was used from 11 h to 17 h when concentration was high. In general, Site 3 showed high concentration. The vehicle is controlled at regular times on weekdays (11-14 h) and Saturdays (10-17 h) at Site 3. Due to traffic volume is low, the  $\text{NO}$  emission that acts as a sink for ozone was restricted, so the ozone concentration seems to be recorded high. The concentration distribution of ozone and  $\text{NO}_2$  has an inverse correlation. In summer, the concentration distribution of ozone tended to be higher in Site 3 than in Site 1 and Site 2 (Fig. 3.6c). Because  $\text{NO}$  emitted from the vehicle is few at Site 3, so the effect of chemical removal of ozone by  $\text{NO}$  is of little. In winter, the concentration difference of  $\text{O}_3$  at each site was very large. The concentration of ozone was significantly higher in Site 1 and Site 3 where the concentration of  $\text{NO}_2$

was relatively low. At Site 2 and Site 4, the concentration of ozone tended to be consistently low, so it was that the effect of  $\text{NO}_x$  that emitted from vehicle emission in the road.

$\text{PM}_{2.5}$  was less concentration differences in each site. Also, when was recorded the low concentration, there were few changes in  $\text{PM}_{2.5}$  concentration during the day. This supports that  $\text{PM}_{2.5}$  is a major production source that secondary generation in the atmosphere rather than primary emissions. In other words,  $\text{PM}_{2.5}$  means that the spatial resolution within 100 m is more affected by a concentration change at a larger scale than the local effect. However, in the high concentration event, not only was the change during the day significantly increased, but the daily average concentration tended to increase significantly compared to other pollutants. In addition, even in a short time of day, the concentration difference was very large (for example, January 12 and 13, January 18 and 19, 20) (Fig. 3.6d). These results suggest the possibility that the effect can be exhibited on a short time scale if the PM pollution policy is implemented appropriately. Choi et al. (2012) obtain to similar conclusions.

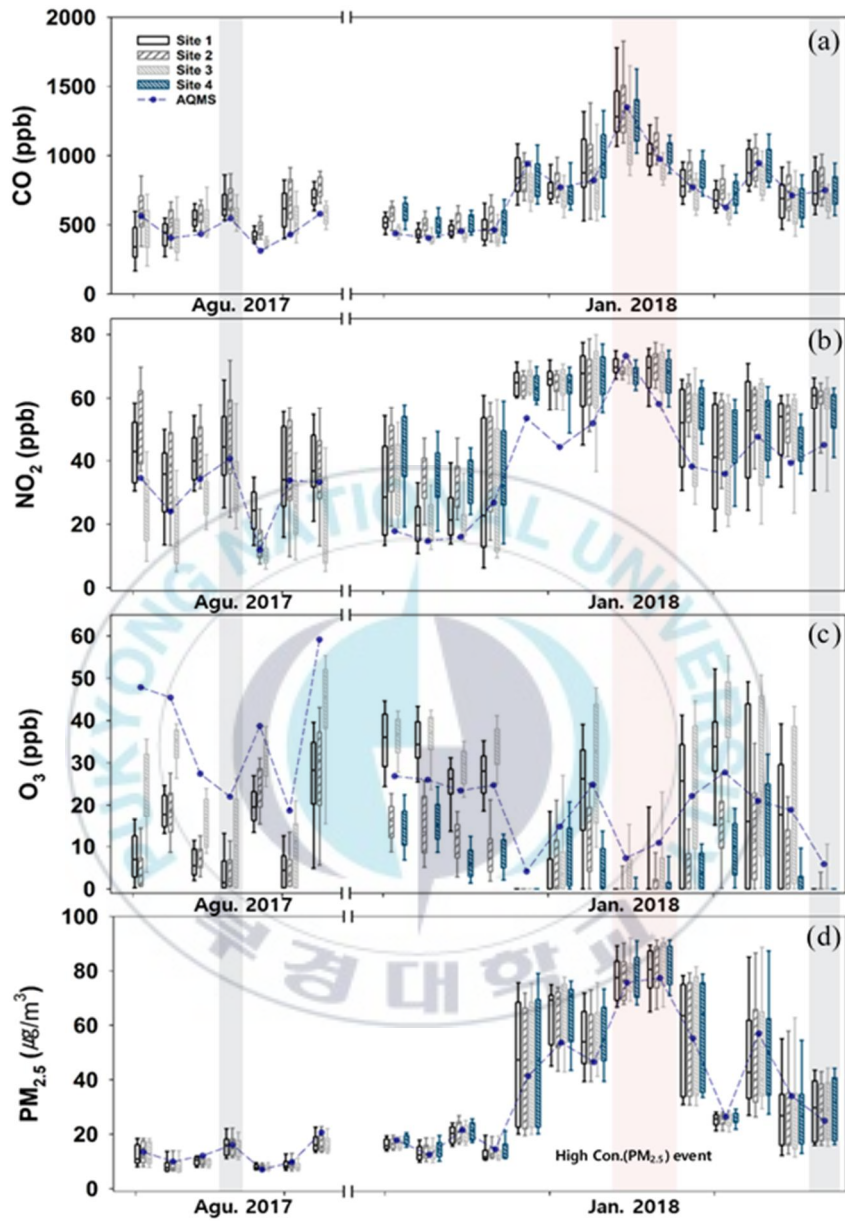


**Fig. 3.6** Box plot of daily changes by measured pollutants by observation area. Each box is the lower 25%, 50%, 75% of the concentration observed during each day in each Site. The gray shaded part represents the day of precipitation. The blue dotted line indicates the average concentration value of AQMS. The red shaded part represents the day of high PM<sub>2.5</sub> concentration event.

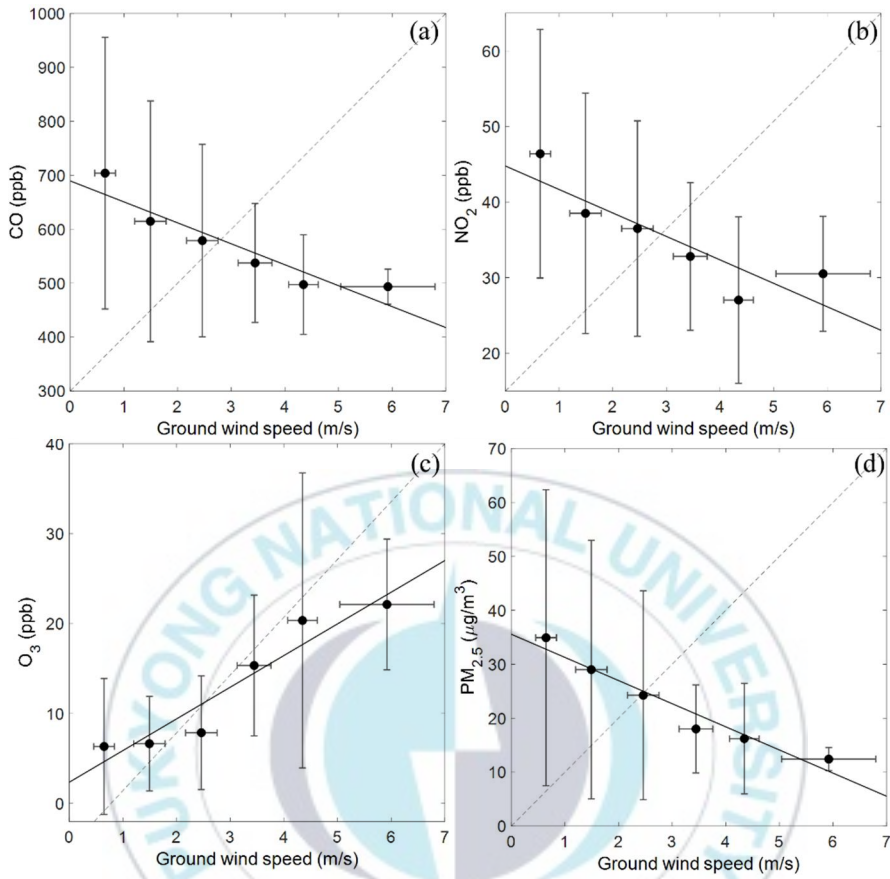


**Fig. 3.7** The wind speed and pollutants concentration comparison when the ground wind direction and the upper wind direction coincide with the road direction (the wind speed comparison plot that when the wind direction coincides with the north wind and the northwest wind in winter (considering monsoon, except high PM<sub>2.5</sub> con. Day and weekend). (a) CO, (b) NO<sub>2</sub>, (c) O<sub>3</sub>, (d) PM<sub>2.5</sub>.

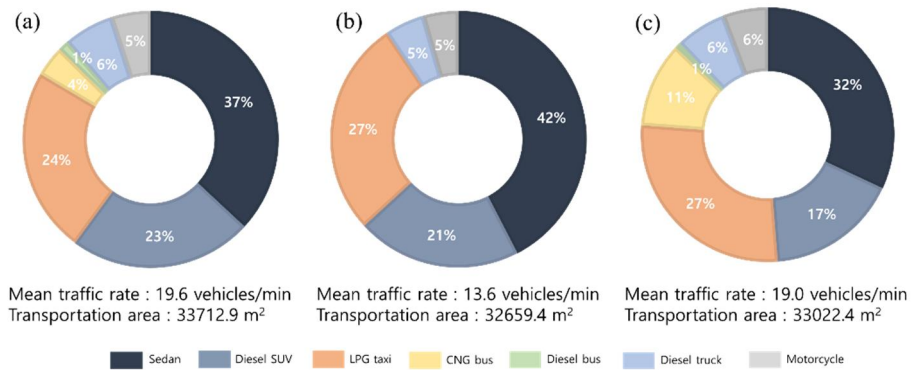


**Fig. 3.8** The average between summer and winter traffic fleet on weekdays. (a) Site1, (b) Site2, (c) Site4.



Changes in the daily concentration of CO, which is the primary pollutant by observation section around the weekday road network showed peaks in the work hours, decreased in the afternoon, and then increased again in the evening (Fig. 3.9-10a). NO<sub>2</sub> also showed a similar weekday change pattern to CO. The difference from CO was that the second peak increased again around 3 pm (Fig. 3.9). This is due to ozone reduction.

The concentration was consistently similar throughout the day at Site 2 and Site 1, but at Site 3, the difference was less than 5 ppb. However, at rush hour, the difference increases more than twice in the afternoon. The NO<sub>2</sub> concentration at night was similar to that at the morning, due to the accumulation of NO<sub>2</sub> formed by the reaction of ozone and NO at night in the absence of ultraviolet light.

O<sub>3</sub> showed the low concentration at the time of commencement, and then increased rapidly at around 11 am, recording the first highest concentration at around 2 pm, and then decreasing and showing the second highest concentration peak at around 5 pm (Fig. 3.9c). The first increase was due to formation through a local photochemical process, and second peaks appear to be due to the transfer of air, including ozone, formed in the surrounding area. The overall low ozone concentration, even in summer, seems to be due to the chemical removal effect due to the continuous inflow of NO emitted from the vehicle.

PM<sub>2.5</sub> showed a difference of up to about 6 µg/m<sup>3</sup> in the daily change, so the effect of work time was not strong (Fig. 3.9-10d). The peculiarity of the change in winter is that the increase only in Site 4 at 12 pm and 6-7 pm (Fig. 3.10d). Considering that the restaurant streets are densely distributed around Site 4, there is



a possibility that the PM emission from the catering industry is similar to the road effect. Therefore, there is a need for further research on the effect of PM emissions from restaurant districts on the increase in local PM concentration.



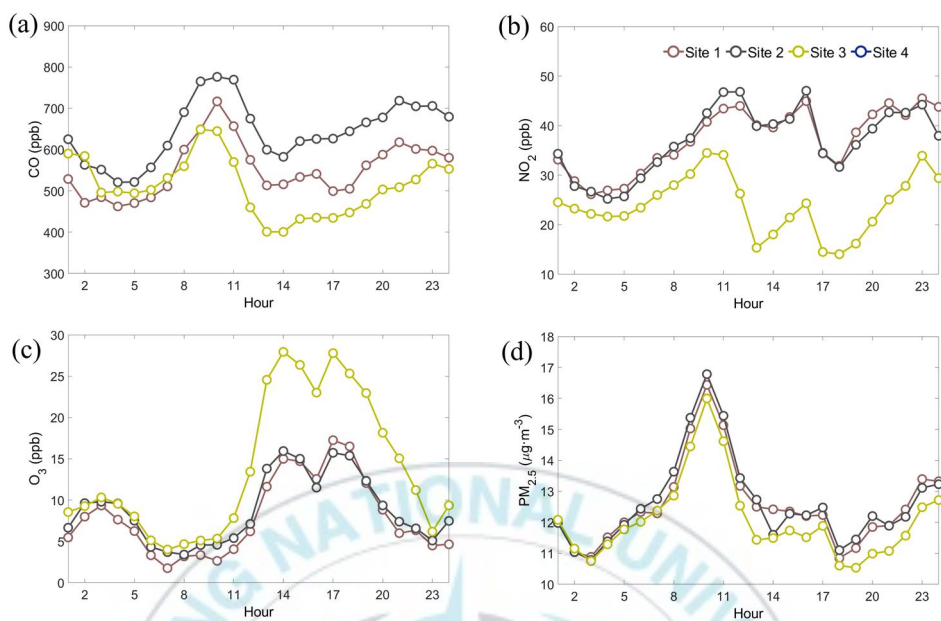


**Fig. 3.9** Daily variation of contaminants in Site 1 (brown), Site 2 (black), and Site 3 (yellow-green) over the weekday summer observation period (1 hour avg). (a) CO; (b) NO<sub>2</sub>, (c) O<sub>3</sub>; and (d) PM<sub>2.5</sub>.

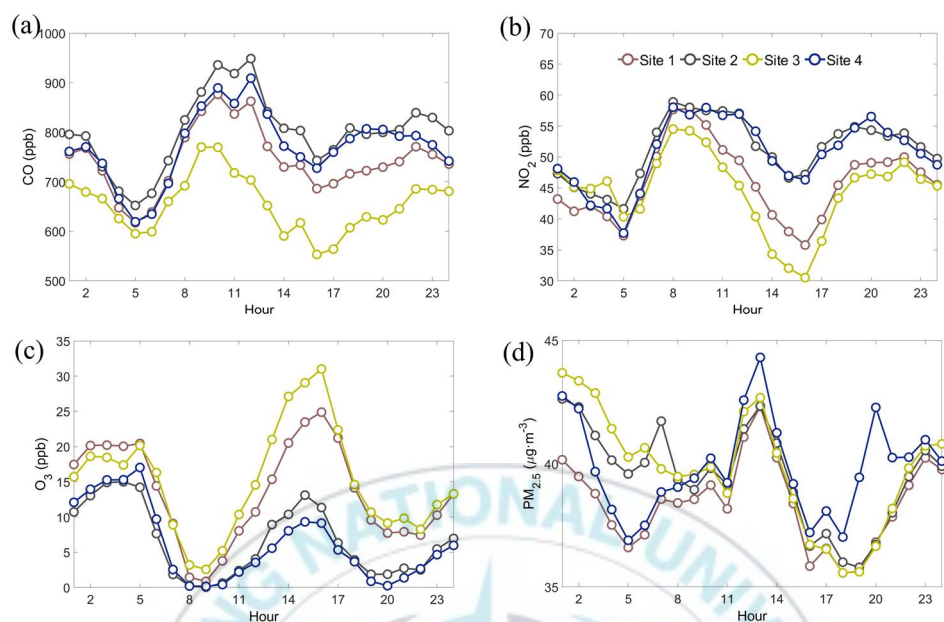


**Fig. 3.10** Daily variation of pollutants in Site 1 (brown), Site 2 (black), Site 3 (yellow-green), and Site 4 (blue) over the weekday winter observation period (1 hour avg). (a) CO; (b) NO<sub>2</sub>, (c) O<sub>3</sub>; and (d) PM<sub>2.5</sub>.

### 3.4. Spatial variability

The concentration distribution of pollutants showed a difference in temporal and spatial, and the difference was different for each pollutant. To determine the temporal and spatial variability of the paired sites (Site1 - 4), two coefficients were used the coefficients of Pearson's correlation (R) and coefficient of divergence (COD). COD can be used to analyze concentration and spatial variability of mass by size at a pair of sites (e.g., Site1, Sit2) at concentrations measured simultaneously on a specific date (Wilson et al., 2005). The COD is calculated as follows.

$$COD = \sqrt{\frac{1}{n} \sum_{i=1}^n \left( \frac{x_{if} - x_{ih}}{x_{if} + x_{ih}} \right)^2} \quad (\text{Eq. 3.1})$$

n is the number of observations, f and h are two observation site to be compared, and  $x_f$  and  $x_h$  are pollutant concentrations in site, respectively. When the COD is 0, the two observation points can be homogeneous, and if it is 0.20 or more, it can be regarded as spatially very heterogeneous (Moore et al., 2009; Wilson et al., 2005). In this study, the days of high concentration and precipitation were excluded (Fig. 3.6, shaded box), and the daily concentrations at 1 hour intervals were calculated COD and R based on Site 3, which can be seen as the background concentration (Fig. 3.11).

CO was between 0.02 - 0.21 and correlation was between 0.29 - 0.98. Most of the COD values were 0.2, but R values were large (Fig. 3.11a). CO is a pollutant with a long lifetime of several weeks to several months (Holoway et al., 2000), and it is difficult to see the difference in concentration of each road due to the CO emitted directly from the car and the residual CO. It is more affected by wind speed and direction (Fig. 3.7a).

NO<sub>2</sub> showed a non-homogeneous distribution in summer and a relatively homogeneous distribution in winter (COD: 0.04 - 0.57, R: 0.12 - 0.98). In winter, the concentration difference by site is generated by a similar source, but there is a concentration size difference (Fig. 3.9b). O<sub>3</sub> showed a heterogeneous distribution in both summer and winter (COD: 0.15 - 0.71, R: -0.06 - 0.98).

The mass concentration of PM<sub>2.5</sub> showed a homogeneous distribution (COD: 0.02 - 0.11, R: 0.94 - 0.99, Fig. 3.11d). As seen in the time series of PM<sub>2.5</sub>, the mass concentration is more affected by external sources than local sources. This result is consistent with the results of other studies. However, the composition of chemical components in PM<sub>2.5</sub> showed homogeneous in each site (Krudysz et al., 2008). In the experiments conducted in Los Angeles, the spatial distribution of mass concentration and OC concentration was mostly homogeneous but showed heterogeneous distribution such as EC and quasi-UF (Krudysz et al., 2008). In conclusion, the distribution of mass concentration has a homogeneous distribution in site, but the spatial distribution of chemical components varies depending on the source in the site.

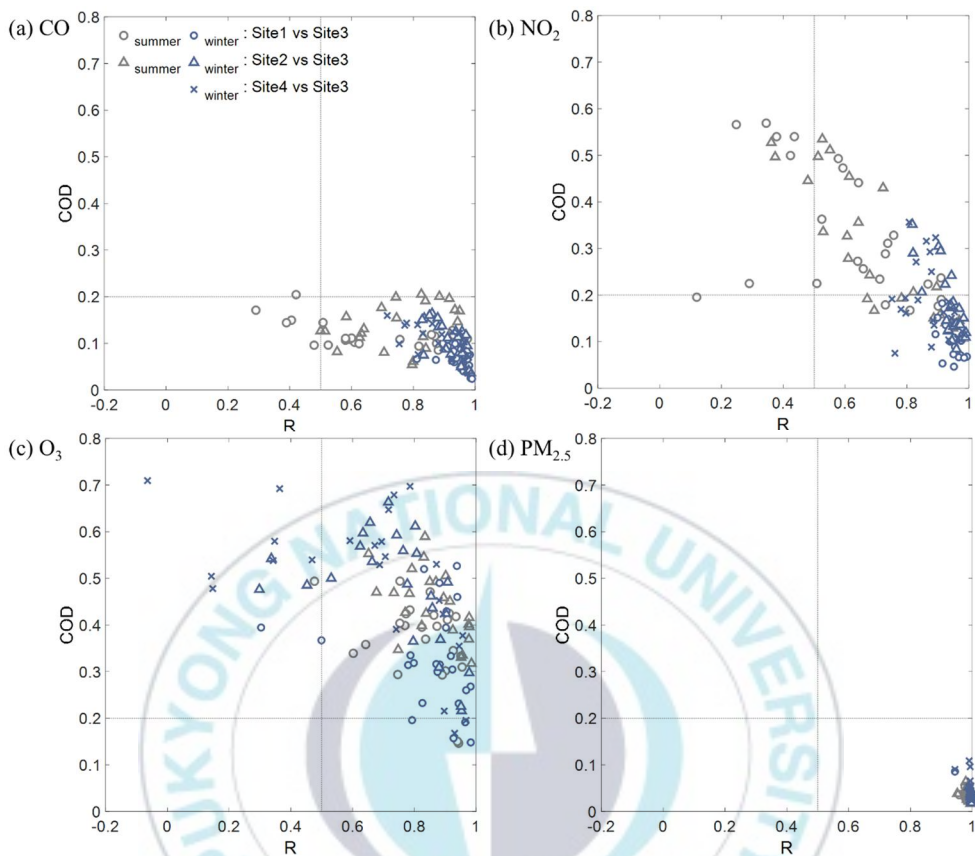


**Fig. 3.11** A daily (24h) COD distribution with a concentration of pollutants using 1 h data in observe periods (except for the day when precipitation and high concentrations occurred). Based on Site 3, the circle is the comparison of Site 1, Site 2, Site 2, and the product table, Site 4. Gray is the summer observation and blue are the winter observation. (a) CO, (b) NO<sub>2</sub>, (c) O<sub>3</sub>, (d) PM<sub>2.5</sub>.

### 3.5. Summary

In this study, low-cost sensors were used to measure in four site with different environments. The wind speed in urban showed a relatively strong wind speed if the direction of the road and wind direction were matched (slope: 1.8 (in summer), 1.9 (in winter)). These results also affected the concentration distribution. CO, NO<sub>2</sub>, and PM<sub>2.5</sub> showed the inverse relationship of ozone when the wind direction was in line with the road direction, the stronger the wind speed, the higher the diffusion efficiency. CO tended to decrease by 39 ppb s/m, NO<sub>2</sub> 3 ppb, PM<sub>2.5</sub> 4 µg/m<sup>3</sup> as the wind speed per 1 m/s became stronger, and ozone tended to increase by 3 ppb.

In COD analysis of air pollutants, most pollutants except PM<sub>2.5</sub> showed considerable heterogeneous in distribution in time and space. The COD value of CO was between 0.02 - 0.21, and the correlation value was 0.29 - 0.98, indicating a moderate heterogeneity within the site. This has significantly reduced emissions from traffic due to recent policies, which seem to be relatively less affected by other pollutants. NO<sub>2</sub> showed a heterogeneous distribution in summer and a relatively homogeneous distribution in winter (COD: 0.04 - 0.57, R: 0.12 - 0.98). NO<sub>2</sub> is directly affected by various regional sources. O<sub>3</sub> showed the most heterogeneous distribution between pollutants due to chemical reaction with NO<sub>x</sub>. PM<sub>2.5</sub> showed very homogeneous distribution within the detailed scale (COD < 0.2). Rather than being affected by direct emissions with highly resolved, PM<sub>2.5</sub> have been more affected by



the secondary generation of the atmosphere on a regional scale and inflow by long-distance transport. Thus, the impact of direct emissions from local traffic is limited. However, the amount of inhalation by pedestrians differed depending on the conditions.

CO has a relatively homogeneous distribution in space and time in the detailed area due to the decrease in the concentration emitted from road-moving pollutants due to recent traffic reduction policies. However, although smaller than the overall trend of change, there was a difference in the CO concentration in each observation site, showing that the influence of the above-ground wind field was somewhat.

NO<sub>2</sub> showed that the direct effect of various local emission sources was non-homogeneous in spatial-temporal distribution, and the distribution of ozone was different due to the rapid chemical reaction with NO<sub>x</sub> emitted from road transport sources in each region. PM<sub>2.5</sub> showed a very homogeneous spatial distribution within the detailed area and appears to be more affected by secondary generation in the atmosphere at the regional scale and influx by long-distance transport than by direct emissions.

However, previous studies have shown that although the mass concentration may be homogeneous, the chemical composition or number concentration shows an heterogeneous distribution in the small-scale site (Massoud et al., 2011), and further study is needed.

## CHAPTER 4

### CONCLUSIONS

This study showed the concentration distribution in highly resolved site using low cost sensors and suggested the possibility of establishing public transportation guidelines to minimize exposure to  $PM_{2.5}$  in specific conditions. These results can improve the accuracy of urban modeling. Also, we can be used as a basis for the development of an air pollution exposure evaluation model considering distance, means and time of movement with a given external  $PM_{2.5}$  concentration condition. However, this study is based on observations for a relatively short period and the weather environment required for some assumptions is incomplete, so further research is required to calculate more reliable emissions. Also, this study is limited to spring and summer, so it is required to accumulate data through additional measurements of late autumn and winter with high concentration of  $PM_{2.5}$  in the atmosphere.

If additional studies can such as analysis of difference in exposure intake if the bus stop is in the middle of the road or the sidewalk is wide, it is expected to help develop a more specific location/behavioral exposure risk assessment model. And if continuous observations are accompanied in the area with the appropriate weather environment in the urban, the possibility of evaluating the emission from vehicle based on observations.

## REFERENCE

- Baumgartner J., Zhang Y., Schauer J.J., Wei H., Wang Y., Ezzati M. (2014) Highway proximity and black carbon from cookstoves as a risk factor for higher blood pressure in rural China, *Proceedings of the National Academy of Sciences of the United States of America*, 111 (36): 13229-13234.
- Bentayeb M., Wagner V., Stempfelet M., Zins M., Goldberg M., Pascal M., Larrieu S., Beaudeau P., Cassadou S., Eilstein D., Filleul L. (2015) Association between long-term exposure to air pollution and mortality in France: a 25-year follow-up study, *Environment International*, 85: 5–14.
- Britter RE., Hanna SR. (2003) Flow and dispersion in urban areas, *Annual Review of Fluid Mechanics*, 35: 469–496
- Busan Metropolitan City (BMC) (2019) 2018 Traffic Analysis in Busan Metropolitan City (I), Busan Metropolitan City, Korea, <https://www.busan.go.kr/bhstatistics10> (last access on 6/10/2020), (in korean).
- Choi, W., He, M., Barbesant, V., Kozawa, K. H., Mara, S., Winer, A. M., Paulson, S. E. (2012) Prevalence of wide area impacts downwind of freeways under pre-sunrise stable atmospheric conditions, *Atmospheric Environment*, 62: 318-327.

- Choi, W., Hu, S., He, M., Kozawa, K., Mara, S., Winer, A. M., Paulson, S. E. (2013) Neighborhood-scale air quality impacts of emissions from motor vehicles and aircraft, *Atmospheric Environment*, 80: 310-321.
- Choi, W., Kim, J. (2018) Characteristics of Ultrafine Particles in Urban Areas Observed Worldwide and in Korea: Sources and Emissions, Spatial and Temporal Distributions, and Health Effects, *Korean Meteorological Society*, 28 (3): 337-355, (in Korean with English abstract).
- Choi, W., Ranasinghe, D., DeShazo, J., Kim, J., Paulson, S. E. (2018) Where to locate transit stops: Cross-intersection profiles of ultrafine particles and implications for pedestrian exposure, *Environmental pollution*, 233: 235-245.
- Cordero, J.M.; Borge, R.; Narros, A. (2018) Using statistical methods to carry out in field calibrations of low cost air quality sensors, *Sensors and Actuators B: Chemical*, 267: 245–254.
- Fusi, S., Cutuli, D., Valente, M., Bergonzi, P., Porro, C. A., Di Prampero, P. (2005) Cardioventilatory responses during real or imagined walking at low speed, *Archives italiennes de biologie*, 143 (3-4): 223-228.
- Goel, A., Kumar, P. (2015) Characterisation of nanoparticle emissions and exposure at traffic intersections through fast–response mobile and sequential measurements, *Atmospheric Environment*, 107: 374-390.

- Hoek G., Krishnan R.M., Beelen R., Peters A., Ostro B., Brunekreef B., Kaufman J.D. (2013) Long-term air pollution exposure and cardiorespiratory mortality: a review, *Environmental Health*, 12 (1): 43.
- Holloway, T., H. Levy II, and P. Kasibhatla (2000) Global distribution of carbon monoxide, *Journal of Geophysical Research*, 105:12,123-12,147.
- Kerminen, V. M., Coauthors, (2007) Development of particle number size distribution near a major road in Helsinki during an episodic inversion situation. *Atmospheric Environment*, 41: 1759-1767.
- Kim, M. k., Cha, Y. W., Lee, S. L., Yoo, E. C. (2014) Study on the Secondary Formation Contribution of PM in Busan, *The Annual Report of Busan Metropolitan City Institute of Health & Environment*, 24(1): 146-160, (in Korean with English abstract).
- Krudysz, M.A., Froines, J.R., Fine, P.M., Sioutas, C. (2008) Intra-community spatial variation of size-fractionated PM mass, OC, EC, and trace elements in the Long Beach, CA area, *Atmospheric Environment*, 42: 5374-5389.
- Kumar, P., A. Robins, S. Vardoulakis, and R. Britter (2010) A review of the characteristics of nanoparticles in the urban atmosphere and the prospects for developing regulatory controls, *Atmospheric Environment*, 44 (39): 5035-5052.
- Kumar, P., Ketzel, M., Vardoulakis, S., Pirjola, L., Britter, R. (2011b) Dynamics and dispersion modelling of nanoparticles from road traffic in the urban atmospheric environment-A review, *Journal of Aerosol Science*, 42: 580-603.

- Lee H.D., Park C.G. (2019) Characteristic analysis of quantitative concentration and particle counter of particular matter in Seoul subway station, Proceedings of the Korean Society for Fluid Machinery Annual Meeting 2019.7: 303-305
- Lee, J., Byeon, S., Lee, J. (2009) The effect of platform screen door (PSD) for fine particles at subway train in Seoul, Korea, ICROS-SICE International Joint Conference 2009, Aug. 18-21, Fukuoka, Japan, IEEE: 1707-1710.
- Massoud, R., Shihadeh, A.L., Roumié, M., Youness, M., Gerard, J., Saliba, N., Zaarour, R., Abboud, M., Farah, W., Saliba N.A. (2011) Intraurban variability of PM10 and PM2.5 in an Eastern Mediterranean city, *Atmospheric Research*, 101: 893-901
- Mead, M.I., Popoola, O.A.M., Stewart, G.B., Landshoff, P., Calleja, M., Hayes, M., Baldovi, J.J., McLeod, M.W., Hodgson, T.F., Dicks J., Lewis A., Cohen J., Baron R., Saffell J.R., Jones R.L. (2013) The use of electrochemical sensors for monitoring urban air quality in low-cost, high-density networks, *Atmospheric Environment*, 70: 186-203
- Ministry of Environment (ME) (2016) We can understand it if we know correctly: Fine particles, what is it?, Ministry of Environment (ME), Sejong City, <http://www.me.go.kr/daegu/web/board/read.do?menuId=724&boardId=629480&boardMasterId=167&condition.hideCate=1> (last access on 6/10/2020), (in korean).

- Moore, K., Krudysz, M., Pakbin, P., Hudda, N., Sioutas, C. (2009) Intra-community variability in total particle number concentrations in the San Pedro Harbor area (Los Angeles, California), *Aerosol Science and Technology*, 43 (6): 587-603.
- Morawska, L., Ristovski, Z., Jayaratne, E., Keogh, D. U., Ling, X. (2008) Ambient nano and ultrafine particles from motor vehicle emissions: Characteristics, ambient processing and implications on human exposure, *Atmospheric Environment*, 42: 8113-8138.
- National Institute of Environment Research (NIER) (2009) A Study on management of non-regulated indoor air pollutant in Korea ( I ): PM2.5, ammonia, <http://webbook.me.go.kr/DLi-File/NIER/06/013/5254313.pdf> (in korean).
- National Institute of Environment Research (NIER) (2017) A Study on developing highly-resolved air pollutant emissions by air pollution forecasting district ( I ), in review (in korean).
- National Institute of Environment Research (NIER) (2019) A Study on management of non-regulated indoor air pollutant in Korea ( I ): PM2.5, ammonia, <http://webbook.me.go.kr/DLi-File/NIER/06/013/5254313.pdf> (in korean).
- National Institute of Environment Research (NIER) (2019) Air Pollution Monitoring Network Installation and Operation Guidelines (2019), <https://ecolibrary.me.go.kr/nier/#/search/detail/5671447> (last access on 6/10/2020), (in korean).



- Park, D., Ha, K. (2008) Characteristics of PM<sub>10</sub>, PM<sub>2.5</sub>, CO<sub>2</sub> and CO monitored in interiors and platforms of subway train in Seoul, Korea, *Environment International*, 34: 629-634.
- Park, H.S., Kim, R.E., Park, Y., Hwang, K.C., Lee, S.H., Kim, J.J., Choi, J.Y., Lee, D.G., Chang, L.S., Choi, W. (2020) The Potential of Commercial Sensors for Spatially Dense Short-term Air Quality Monitoring Based on Multiple Short-term Evaluations of 30 Sensor Nodes in Urban Areas in Korea, *Aerosol and Air Quality Research*, 20: 369–380.
- Sioutas, C., Delfino, R. J., Singh, M. (2005) Exposure Assessment for Atmospheric Ultrafine Particles (UFPs) and Implications in Epidemiologic Research, *Environmental Health Perspectives*. 113 (8): 947-955.
- Spinelle L., Gerboles M., Gabriella Villani M., Aleixandre M., F. Bonavitacola F. (2015) Field calibration of a cluster of low-cost available sensors for air quality monitoring. Part A: ozone and nitrogen dioxide, *Sensors and Actuators B: Chemical*, 215: 249-257.
- Tan, Y., Lipsky, E. M., Saleh, R., Robinson, A. L., and Presto, A. A. (2014) Characterizing the Spatial Variation of Air Pollutants and the Contributions of High Emitting Vehicles in Pittsburgh, PA, *Environmental Science & Technology*, 48: 14186–14194.
- TSI (2019) DUSTTRAK™ II Aerosol monitor operation and service manual, TSI Inc., Shoreview, MN, <https://www.tsi.com/getmedia/7c608b93-b6d1-459a-a6a8->

2b0e2a55ba91/8530-8531-8532-DustTrak\_II-6001893-web?ext=.pdf (last access on 6/10/2020).

Vachon, G., Louka, P., Rosant, J.-M., Mestayer, P., Sini, J.-F. (2002) Measurements of traffic-induced turbulence within a street canyon during the Nantes '99 experiment, *Water, Air and Soil Pollution: Focus volume*, 2: 127–140.

Wang, X. R., Gao, H. O. (2011) Exposure to fine particle mass and number concentrations in urban transportation environments of New York City, *Transportation Research Part D: Transport and Environment*, 16 (5): 384-391.

Wilson, J.G., Kingham, S., Pearce, J., Sturman A.P. (2005) A review of intraurban variations in particulate air pollution: implications for epidemiological research, *Atmospheric Environment*, 39 (34): 6444.

Wu S., Ni Y., Li H., Pan L., Yang D., Baccarelli A., Deng F., Chen Y., Shima M., Guo X. (2016) Short-term exposure to high ambient air pollution increases airway inflammation and respiratory symptoms in chronic obstructive pulmonary disease patients in Beijing, China, *Environment International*, 94: 76-82.

Xing, Y. F., Xu, Y. H., Shi, M. H., Lian, Y. X. (2016) The Impact of PM<sub>2.5</sub> on the Human Respiratory System, *Journal of Thoracic Disease*, 8 (1): E 69-74.

Zacharias, A., Masterson, T., Kim, K. (2014) The measurement of time and income poverty in Korea, Levy Institute Research Project Report, Levy Economics Institute of Bard College, Annandale-On-Hudson, New York, <http://www.levyinstitute.org/publications/the-measurement-of-time-and-income->

poverty-in-korea-the-levy-institute-measure-of-time-and-income-poverty (last access on 7/01/2020).

Zhu, Y., Eiguren-Fernandez, A., Hinds, W. C., Miguel, A. H. (2007) In-cabin commuter exposure to ultrafine particles on los angeles freeways, *Environmental science & technology*, 41: 2138-2145.

